CODEN:LUTEDX/(TEIE-5516)/1-83/(2024)

Industrial Electrical Engineering and Automation

Impact on the Technical Performance of a Utility-Scale PV Plant when Using Different Sizes and Numbers of Transformers

Jens Elfström
Oliver Lindblom

Division of Industrial Electrical Engineering and Automation
Faculty of Engineering, Lund University

Master Thesis

Impact on the Technical Performance of a Utility-Scale PV Plant when Using Different Sizes and Numbers of Transformers

by

Jens Elfström & Oliver Lindblom

LUND UNIVERSITY

LTH

FACULTY OF ENGINEERING

REJLERS

Factulty of Engineering LTH at Lund University

Divsion of Industrial Electrical Engineering and Automation

Supervisor: **Max Collins (IEA, LTH)**

Industry Supervisor: **Victor Lovén (Rejlers Sverige AB)**

Examiner: **Jörgen Svensson (IEA, LTH)**

June 12, 2024

Abstract

The main focus of this thesis has been to examine and compare how the size and number of internal power transformers affects the technical performance (robustness, power quality and efficiency) of a utility-scale PV plant. The technical performance was examined in a simulation environment (MATLAB Simulink), where a PV plant with a fixed number of PV arrays and converters, corresponding to a rated power of 40 MW, was connected to the grid in four different ways, resulting in four simulation models. First off two models, using 4 x 10 MVA transformers respectively 20 x 2 MVA transformers, were built and simulated under different site conditions (grid strength and distance to PCC) and disturbances (varying solar irradiation and grid frequency). The simulations showed no significant performance difference between the two models.

Further, two more models, using 1 x 40 MVA transformer and 40 x 1 MVA transformers, were introduced as the first two showed no difference in performance. These, along with the old models, were then stress tested in order to get further indications if the size and number of transformers affects the performance, and now more specifically the robustness of a PV plant. The stress test was performed by decreasing the grid strength until the control systems no longer could follow their set-points. This corresponds to the system no longer being stable. The stress test showed small differences between the robustness of the four models, but no correlation between the number of transformers and robustness was observed.

As a whole the simulations showed that the size and number of transformers had no significant impact on the technical performance of the PV plant. In addition to the technical simulations, a brief qualitative economical comparison, between using a few large versus many small transformers was conducted. The comparison was made in three aspects; components and labour, logistics and reliability/redundancy. Regarding the amount of components and labour needed, using a few large transformers was clearly favorable. The logistical aspect was very case dependent and could favor either many small or a few large. In terms of reliability and redundancy many small transformers was favorable.

Preface

This thesis, for the degree of Master of Science in Electrical Engineering, has been carried out at the Department of Industrial Electrical Engineering and Automation (IEA) at the Faculty of Engineering at Lund University (LTH) in collaboration with Rejlers Sverige AB.

First off we would like to thank Rejlers Sverige AB for the opportunity to write this thesis in collaboration with them and for coming up with the idea on which the work is based. In particular we want to thank our supervisor Victor Lovén for support, interesting discussions and valuable input through the whole work process. We would also like to acknowledge all other people at Rejlers who shared valuable knowledge and engaged in the work, including Simon Harnestam.

We also want to express our gratitude to our supervisor Max Collins at IEA for sharing a portion of his expertise in power electronics, helping with complicated simulations problems and overall supporting words.

Terminology and Abbreviations

DG - Distributed generation

GSU - Generator step-up

LF - Loop Filter

MPPT - Maximum Power Point Tracking

PCC - Point of Common Coupling

PD - Phase Detector

PF - Power Factor

PLL - Phase-locked loop

PPM - Power Park Module

PV - Photovaltaics

P&O - Perturbation & Observation

PWM - Pulse-width modulation

RFG - Requirements for generators

SCR - Short-Circuit Ratio

THD - Total Harmonic Distortion

VCO - Voltage-Controlled Oscillator

VSI - Voltage-Source Inverter

Contents

1 Introduction

In this master thesis the impact of the number and size of internal transformers on the technical performance, in terms of robustness, power quality and efficiency, of utility-scale photovoltaic (PV) plants is investigated. A brief qualitative economical comparison between using many small or a few large transformers will also be conducted. The technical investigation will be carried out with simulations using MATLAB-Simulink.

The introduction chapter starts by providing a background for the work in terms of the world transitioning towards renewable energy, the expansion of utility-scale PV plants and the use of transformers in utility-scale PV plants. A problem formulation based on this follows and from it the research goals of this thesis are formulated. The last part of the introduction presents the delimitations imposed on this work.

1.1 Background

According to [1] the growth of renewable energy in Europe will more than double in 2023-2028 compared to the previous six years. The same report [1] also states that 70%, of this growth will be in PV of which about 40% is utility scale. What counts as utility-scale is not clearly defined, but in comparison to distributed PV systems it is more large-scale and connects to a higher voltage level. Utility scale PV is dependent on transformers for connecting to the electricity grid, in order to step up the voltage. Grid connected PV power generation started in a smaller scale than what is common today using relatively small transformers. When gradually aggregating into utility-scale PV plants the practice of using small transformers stuck, resulting in utility-scale PV plants commonly being connected using a large number of smaller transformers [2]. At the same time it is hard to find studies evaluating what size and number of transformers should be used.

Small transformers have the advantages of shorter lead times, less weight per transformer, which could mean easier transport, and more redundant systems. Large transformers, on the other hand, are cheaper per unit of rated power, weight less per unit of rated power and result in a system with less components which brings a number of upsides. These trade-offs will be expanded on in Ch. 6.

1.2 Problem Formulation & Research Goals

For a utility-scale PV plant the technical performance is key. Still the effect that using a different number and size of transformers has not been investigated.

This work will, through simulation, investigate how the technical performance of a utility-scale PV plant depends on the size and number of transformers used for the connection and therein:

1. Investigate how the technical performance of the plant differs depending on the size and number of transformers, under different operating conditions.
2. Stress test plant configurations with different sizes and numbers of transformers to quantify their robustness.

The aspects of technical performance that will be considered are robustness, power quality and efficiency.

With the insight from the investigation into the technical performance:

3. Further analysis will be carried out in the form of a brief qualitative economical comparison.

These are the three research goals considered.

1.3 Outline

After this introductory chapter a theory chapter, Ch. 2, follows. It has two parts where the first deals with the theory of utility-scale PV plants and the second deals with matters relating to the technical performance. A methodology chapter, Ch. 3, follows. It describes how the simulations were set up and how the model was built. Results, Ch. 4, presents the results of the simulations in a plain manner. The discussion, Ch. 5, starts with a discussion of the results and continues with a discussion of the methodology. After this a brief qualitative economical comparison, Ch. 6, of the benefits of using a larger number of smaller transformers is weight against those of using a smaller number of large transformers. In Ch. 7 final conclusions are drawn and some ideas for future work are presented.

1.4 Delimitations

Certain delimitations are imposed on the technical analysis. Despite the fact that utility-scale PV plants can be connected in many ways [3] only one design will be used, in which the number of transformers will be varied. As such different inverter setups, filters and control strategies were not considered. The ones selected were done so on the basis of being commonly used. Note, however, that some adjustments are required to accommodate for different numbers of step-up transformers, these adjustments include; the number and dimensions of the cables used from the transformers to the Point of Common Coupling (PCC) and the controller settings.

The technical investigation is the focus of this work. An economical comparison of using different sizes and numbers of transformers is worth its own work and will only be dealt with briefly here.

2 Theory

In this chapter the theory on which the work is built will be presented, including relevant background for building the simulations models. In Sec. 2.1 an overview of utility-scale PV plants will be given as well as a description of the model used. Sec. 2.1.1-2.1.9 then goes into more depth on the different parts of a utility-scale PV plant, while 2.2 deals with relevant concepts and legislation's regarding the technical performance of the system.

2.1 Utility-Scale PV Plants

This paper concerns the connection of a PV plant to the grid. The core function of the connection is to allow the PV plant to supply power to the grid, and to achieve this some functionalities are required. The PV arrays output DC power at some voltage which needs to be conditioned to AC power at some voltage corresponding to the requirements of the grid in question [4].

Large scale PV-plants can be connected in a variety of ways. The connection considered in this work is illustrated in Fig. 1. The blue, dotted lines represent measurement/control signals.

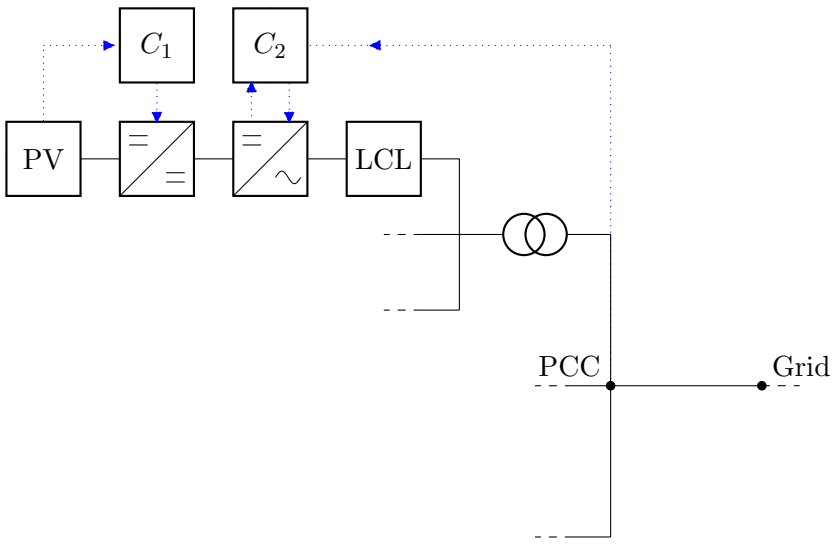

Figure 1: Schematic of a PV plant.

It makes use of a star topology wherein the PCC is connected radially to a number of transformers. Each transformer is then connected radially to a number of branches. The branches consists of an LCL-filter, a DC-AC

converter with its corresponding grid-side controller, C_2, a DC-DC converter with its corresponding input-side controller, C_1, and a PV array [3].

2.1.1 PV Array

On the lowest level the PV arrays consist of PV cells which are interconnected to form PV modules which are, in turn, connected to form PV arrays. In this work the modules are simply viewed as a number of parallel connected strings, where each string consists of a number of series connected PV cells. This is illustrated in Fig. 2 for three parallel strings of four cells each, arbitrarily chosen for this illustration. The modules are connected into arrays in the same way. Connecting cells/modules in series increases the voltage, while connecting cells/modules in parallel increases the current.

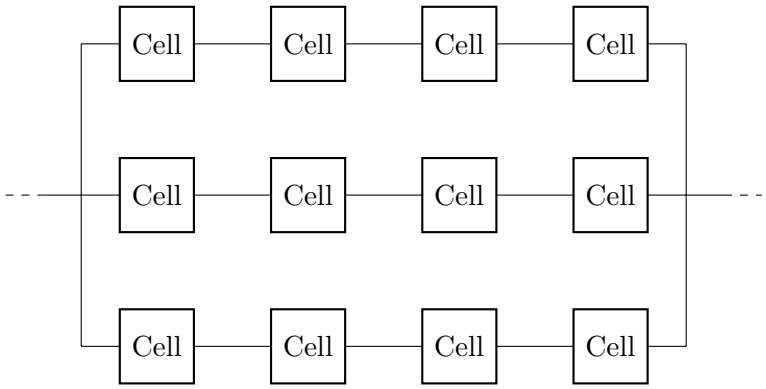

Figure 2: Schematic of a PV module consisting of three parallel connected strings of four cells each.

The cell itself is commonly represented by a single diode model as presented in Fig. 3 [5].

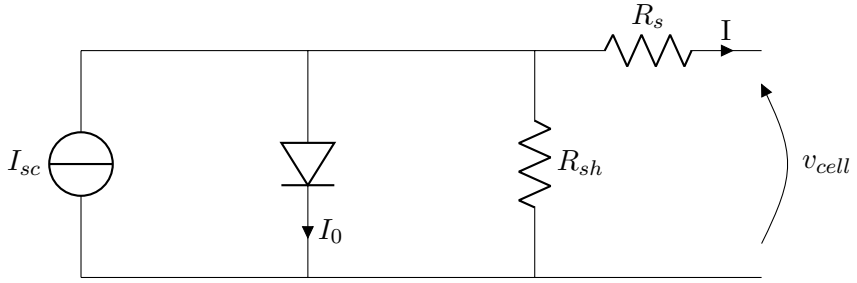

Figure 3: Circuit diagram of a PV cell model.

Nodal analysis on the circuit in Fig. 3 gives the I-V_{cell}, as presented in Eq. 1.

$$I = I_{sc} - I_s \frac{e^{q(V_{cell}+R_s I)}}{BkT} - \frac{V_{cell} + R_s I}{R_{sh}} \tag{1}$$

I_{sc} is the short circuit current, I_s is the reverse saturation current of the diode, q is the elementary charge, B the ideality factor of the junction, k Boltzmanns constant and T the cell temperature. The I-V and P-V relations for a PV array with typical values are illustrated in Fig. 4. Note that the current stays relatively flat as the voltage increases, until a point where it starts falling of quickly. This results in a power peak for the array at approximately the point where the current starts falling off.

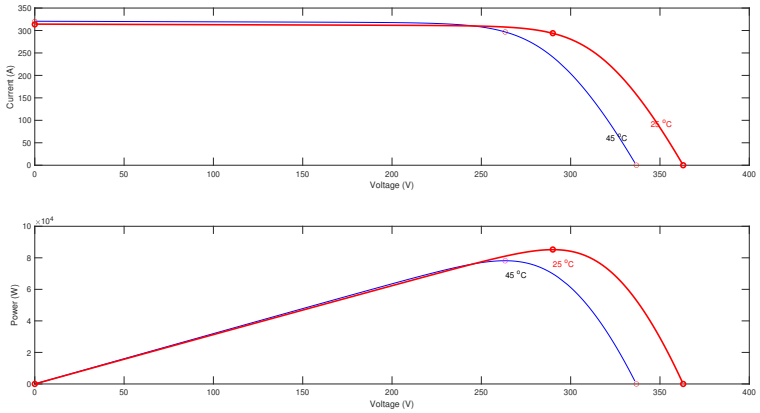

Figure 4: I_{sc}-V and P-V relation.

2.1.2 DC-DC Converter

Since the power varies with the array voltage, as illustrated in Fig. 4, controlling the array voltage becomes of interest. A DC-DC converter can be used to control a varying voltage and is for this reason commonly used in PV connections [6]. A buck converter, illustrated in Fig. 5, is a simple step down converter commonly used for maximum power point tracking (MPPT) of grid connected PV systems [6]. Its operation is controlled via the state of transistor T. In power electronics the transistor is operated in an on-off manner. That is, it is controlled so as to be either almost a short circuit or a open circuit [7]. For high power applications, insulated-gate bipolar transistors (IGBTs) are commonly used with a switching frequency up to 100 kHz [8].

When a PV array is connected on the input and some, more or less constant, load voltage on the output, it is possible to adjust the equivalent load as

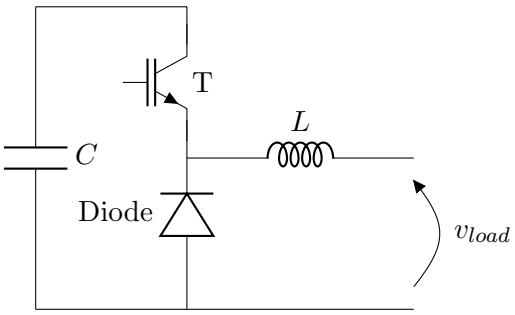

Figure 5: Circuit diagram of DC-DC buck converter.

seen by the PV array by adjusting the duty cycle, the fraction of a switching period that T is conducting. This adjusts the portion of time during which the load is connected to the PV array. In this way the output voltage of the PV array can be controlled and thus the output power can be maximized.

The output inductor L is an integral part of the buck converter. It can be set using Eq. 2 [7].

$$|\Delta i_L| = \frac{v_{load}(1-D)}{L f_{sw}} \tag{2}$$

Δi_L is the current ripple, D is the portion of time during which transistor T is conducting. Solving for L and using the scenario resulting in the largest current ripple, D = 0, gives Eq. 3.

$$L = \frac{v_{load}}{2|\Delta i_L| f_{sw}} \tag{3}$$

As stated in Sec. 2.1.1 the PV array can be seen as a current source, however, the buck converter is a voltage-voltage converter. A capacitor is therefore put on the input of the converter to stabilize the voltage level. For a capacitor Eq. 4 holds.

$$i = C\frac{du}{dt} \tag{4}$$

Approximating $\frac{du}{dt}$ with $\frac{\Delta u}{\Delta t}$, solving for C and considering the case when T is closed gives Eq. 5, which can be used for setting C.

$$C = \frac{I_{mpp} \cdot T_{sw}}{\Delta u} = \frac{I_{mpp}}{\Delta u \cdot f_{sw}} \tag{5}$$

2.1.3 Input-side controller

The aim of the input-side controller is to ensure that the PV plant supplies as much power as possible under varying external conditions, in this case by controlling the buck converter. Multiple MPPT techniques exist to solve this task. However, the most well-known technique according to literature [9] goes under the name Perturbation and Observation (P&O). It is a simple algorithm that works by comparing the PV voltage and power with its previous values and adjusting the duty cycle of the buck converter accordingly. Fig. 6 illustrates a discrete implementation of the algorithm in a flowchart, where $V(k)$ is the voltage at sample k, $I(k)$ is the current at sample k, $P(k)$ is the power at sample k, D is the duty cycle and ΔD is a set perturbation of the duty cycle. The duty cycle is then converted to firing pluses via a pulse-width modulation (PWM) generator for the buck converter. The speed of the algorithm is set by the size of the perturbation and the sampling rate.

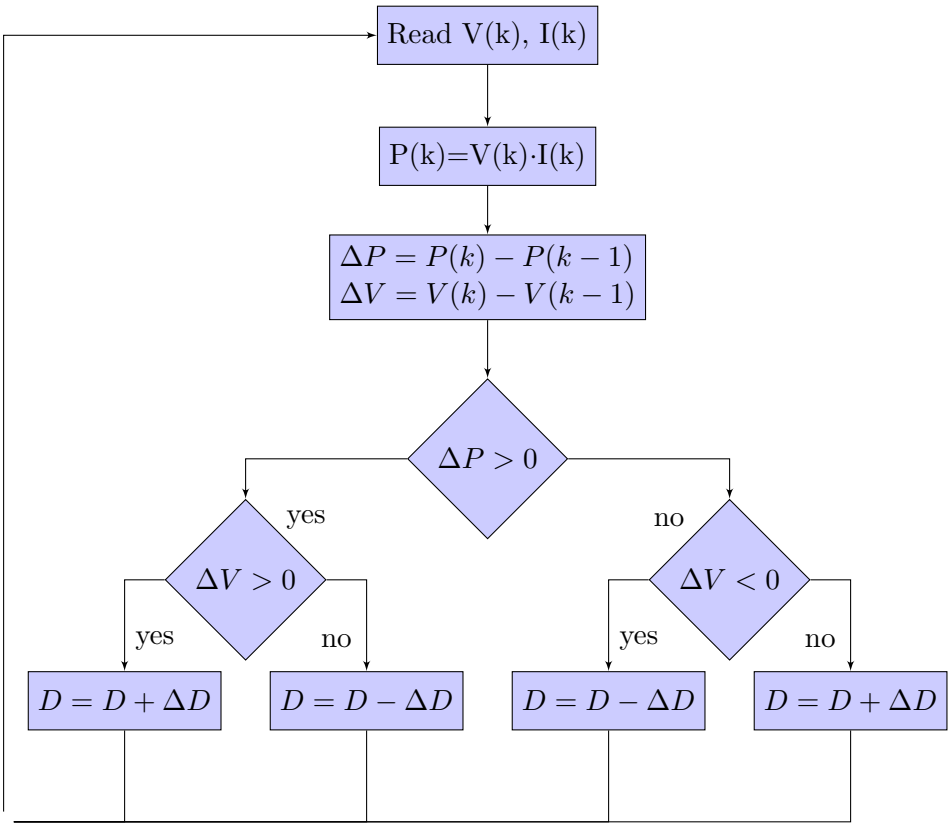

Figure 6: Flowchart of P&O MPPT algorithm.

2.1.4 DC-AC Converter

As stated in Sec. 2.1, the DC power of the PV-cells needs to be converted to AC power to feed the grid. The most commonly used DC-AC converters in grid-connected PV systems are voltage source inverters (VSIs) [10]. The VSI is a bridge circuit made up of legs with power electronic switching devices, one leg for each phase as illustrated in Fig. 7. For a two-level VSI, illustrated in 7, each leg consists of two transistors with one anti-parallel diode each. The converter is driven by a DC voltage along with PWM firing pulses generated by a grid-side controller. As with the buck converter the transistors are operated as switches [7].

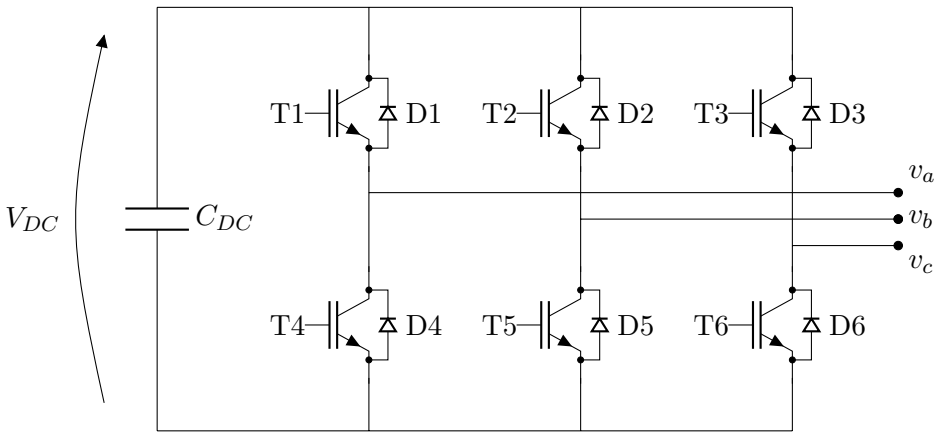

Figure 7: Circuit diagram of a three-phase VSI.

At the input of the inverter, a capacitor, C_{DC}, is placed to reduce DC voltage ripple. It can be sized to limit the ripple of the DC-link voltage to a certain level, ΔV, according to Eq. 6 [11].

$$C_{DC} = \frac{P_{inv}}{2\omega_{grid} V_{DC} \Delta V_{DC}} \tag{6}$$

ω_{grid} is the grid angular frequency and P_{inv} is the power through the VSI.

2.1.5 Grid-Side Controller

The grid-side controller of a PV plant can have many functions, but only the basic ones are considered in this work. These can be divided into three main control tasks; DC link voltage control, active/reactive power injection control and grid synchronization [12]. The DC link voltage is controlled by an outer control loop and active/reactive power is controlled by inner current control loops. The resulting system with plants and controllers is illustrated in Fig. 8. $G_{c,o}$ is the outer controller, $G_{c,i}$ is the inner controller, $G_{p,i}$ is the inner plant and $G_{p,o}$ is the outer plant.

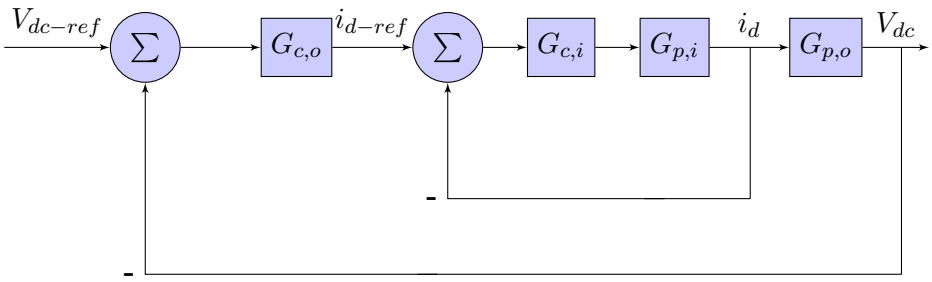

Figure 8: The system consisting of grid side controllers and plants.

The control is done in the DQ reference frame, a framework where the sinusoidal three phase quantities (a, b and c) are transformed into two DC components, known as the direct (d) and the quadrature (q) components. This transformation is achieved using the Park transform, which converts the three-phase sinusoidal signals into a two-axis coordinate system that rotates synchronously with the same frequency as the sinusoidal signals [13]. The transformation depends on the initial alignment of the d-axis and the q-axis. In this work the following is considered; the q-axis is aligned with phase a and the d-axis is aligned 90 degrees behind phase a. Consequently, the transformation is presented in Eq. 7 [13].

$$\begin{bmatrix} d \\ q \\ 0 \end{bmatrix} = \frac{\sqrt{2}}{3} \begin{bmatrix} \sin(\theta) & \sin(\theta - \frac{2\pi}{3}) & \sin(\theta + \frac{2\pi}{3}) \\ \cos(\theta) & \cos(\theta - \frac{2\pi}{3}) & \cos(\theta + \frac{2\pi}{3}) \\ \sqrt{\frac{1}{2}} & \sqrt{\frac{1}{2}} & \sqrt{\frac{1}{2}} \end{bmatrix} \begin{bmatrix} a \\ b \\ c \end{bmatrix} \tag{7}$$

The control is easier achieved in the DQ reference frame, compared to the ABC reference frame, as the reference values are converted from sinusoidally changing ones to constant ones. This allows the use of simple PI-controllers [12]. The DQ frame transform is, however, dependent on synchronizing

with the grid, as it depends on the phase angle from the grid voltages. The synchronization is done through a control system called phase-locked loop (PLL). PLL is an established technique used in many fields of electrical engineering, based on three parts; a Phase Detector (PD), a Loop Filter (LF) and a Voltage-Controlled Oscillator (VCO) [14]. The aim of the PLL system is to extract the phase angle from a periodic input signal. Fig. 9 shows the relationship between the input voltages, V_{abc}, and the output phase angle, θ_0, of the PLL system in a block diagram. PLL algorithms come in many different forms, but the general concept is as follows: The PD computes the phase difference between the input and the output. Further, the LF processes the phase difference, and in turn outputs a control signal to the VCO. The VCO alters its output frequency, and as such alters θ_0, based on its input control signal. In essence, the PLL continuously adjusts θ_0, such that it is synchronized with V_{abc}.

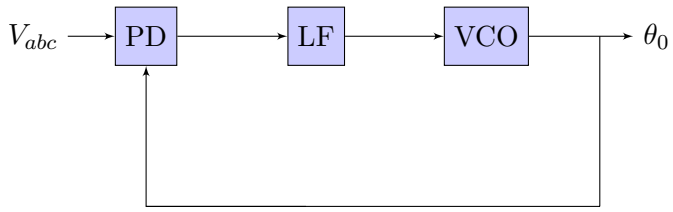

Figure 9: Block diagram of a PLL system.

The block diagram for the inner control loop, $G_{c,i}$, is illustrated in Fig. 10. The inner control loop is usually designed first and then the outer control loop is designed based on it [15]. It consists of two branches. The upper one generates a d-voltage reference for the VSI using a PI controller, which is fed by the d-current error in combination with a feed forward term of the d-voltage of the grid and a cross-coupling term.

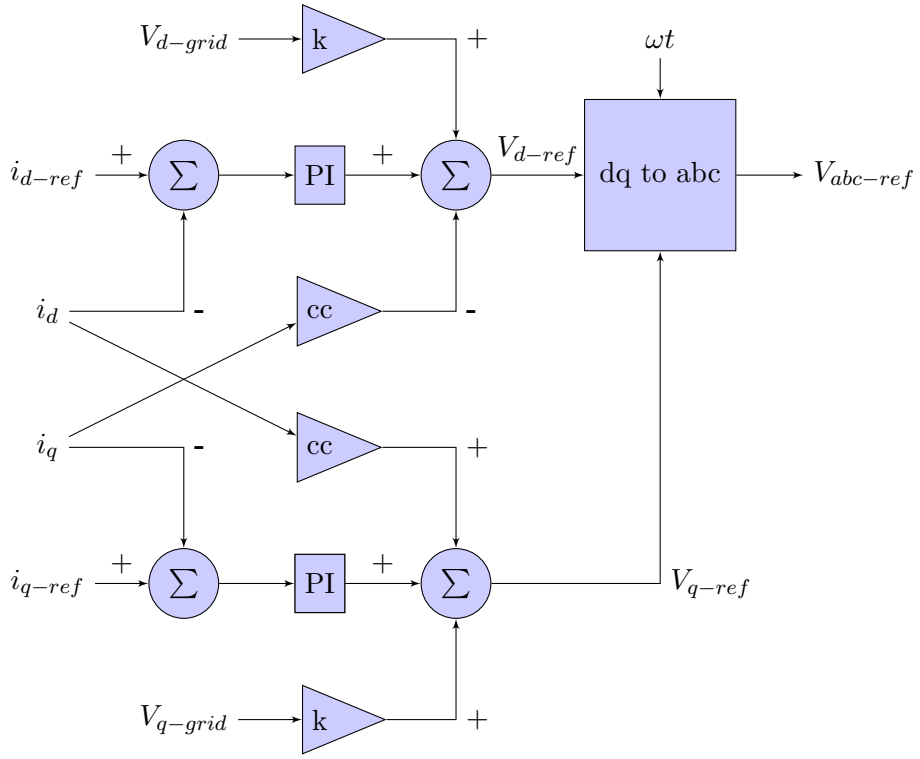

Figure 10: Block diagram of the inner control loop of the grid-side controller.

For the parameters of the PI-controller; direct synthesis is a straight forward method of controller design based on the system dynamics [16]. The current dynamics can be modelled as illustrated in Fig. 11. First, the system is divided into two parts, the transistors and the passive components. The dynamics of the former is much faster than that of the later [7], thus the passive components will dominate the behaviour and the transfer function will become as in Eq. 8.

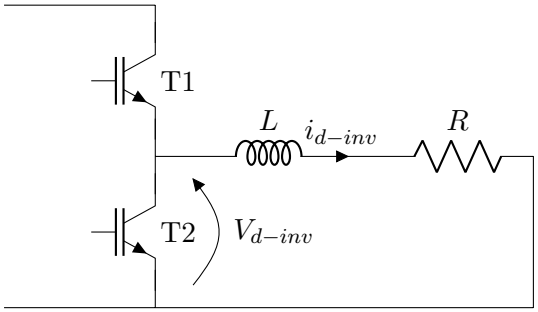

Figure 11: Circuit diagram of a simplified model of the current output of the VSI.

$$G_{p,i} = \frac{i_{d-inv}}{V_{d-inv}} = \frac{1}{sL + R} \tag{8}$$

The system to be controlled is first order, it is then reasonable to equate the closed loop transfer function with $\frac{1}{\lambda_{inner}s+1}$. λ_{inner} is the inverse of the desired system bandwidth. Solving for $G_{c,i}$ yields Eq. 9, a PI controller. In actuality the grid voltage will counteract the inverter d-current, why it is included as a feedforward term with a gain corresponding to the transformer winding ratio $\frac{V_{d-inv}}{V_{d-grid}}$. Additionally the q-current through the impedance will cause a voltage drop which leads the current by 90°, this voltage increase is also included as a negative cross-coupling term.

$$G_{c,i} = \frac{R}{\lambda_{inner}s} + \frac{L}{\lambda_{inner}} \tag{9}$$

The lower branch in Fig. 10 generates the q-voltage reference for the inverter and works in the same way as the upper branch, apart from the fact that the cross-coupling term now is positive.

Further, Fig. 12 illustrates the block diagram for the outer loop of the grid-side controller considered in this work. The upper branch generates the d-current reference using a PI controller, the input of which is the error of the DC-link voltage, combined with a feed forward term of the current into the DC-link capacitor.

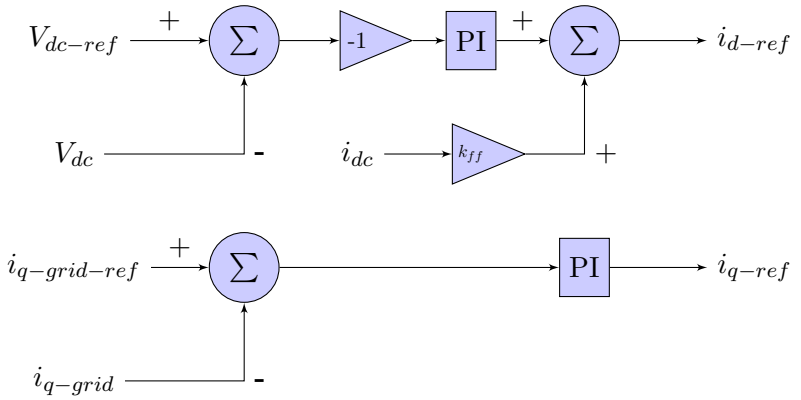

Figure 12: Block diagram of the grid-side controller.

In this case the expression for a typical feedback control system is set up and the controller is solved for. Once again, assuming a first order response for a first order system; $G(s) = \frac{1}{\lambda_{outer}s+1}$ is used as the closed loop transfer

function, where λ_{outer} is the inverse of the desired bandwidth. This yields a expression for the controller. In this case the dynamics between the voltage across a capacitor and the current out of it is given by Eq. 10.

$$\frac{u}{i} = \frac{-1}{Cs} \tag{10}$$

However, in this case the dynamics are the relation between the output voltage of the VSI, and the current into the capacitor. Assuming that the VSI outputs a constant d-voltage and that the dc-link voltage is constant, the transfer function is given by Eq. 11 [17].

$$\frac{u_{dc}}{i_{d-inv}} = \frac{-1}{Cs} \cdot \frac{V_{inv,LL}}{V_{DC}} \tag{11}$$

$V_{inv,LL}$ is the line to line voltage of the VSI output. Equating the closed loop transfer function with $\frac{1}{\lambda_{outer}s+1}$, and solving for $G_{c,o}$ yields Eq. 12 for the controller, a P controller. However, given that this rough model will leave some things out a integral part is added to prevent stationary errors.

$$G_{c,o} = \frac{C}{\lambda_{outer}} \cdot \frac{V_{DC}}{V_{inv,LL}} \tag{12}$$

The system is subject to quite a large disturbance in the form of the current into the capacitor from the buck converter. Since it is easily measured, it can be used as a feed-forward term for i_{d-ref}. Once again this will require a gain of $k_{ff} = \frac{V_{dc}}{V_{inv}}$, for the same reason as with Eq. 12.

The lower branch, in Fig. 12, generates the q-current reference using a PI controller, the input of which is the error of the reactive component of the grid current. This and the d-current reference are then fed into the inner controller, which outputs the voltage references for the VSI. The two voltage references are then transformed into the abc frame and converted into firing pulses for the VSI using PWM.

To avoid system instability, the bandwidths $\frac{1}{\lambda_{outer}}$ and $\frac{1}{\lambda_{inner}}$ should be limited in accordance with some control theory rules of thumb; the inner loop bandwidth should be significantly less than the bandwidth of the process, $\approx \frac{f_{sw}}{10}$, and the outer loop bandwidth should be significantly less than the inner loop bandwidth, $\approx \frac{f_{sw}}{100}$ [18]. The process bandwidth is approximated to the switching frequency, f_{sw}, of the VSI.

2.1.6 LCL-Filter with Damping Resistor

Since power electronic converters output signals containing switching harmonics, the inverter voltage and current waveforms will not resemble pure sinusoidals. Different filter types, with the task of letting through the fundamental frequency and block the switching frequency, exist. A common and economically viable approach is to put an LCL-filter at the inverter output [19]. A single phase LCL-filter in its simplest form consists of an input-side inductor, L_1, followed by a shunt capacitor, C_f and an output-side inductor, L_2, as seen in Fig. 13. Included are also the parasitic resistances of the inductors, r_1 & r_2, along with a damping resistor R_f. The reason for including a damping resistor is that LCL-filters introduce a resonance peak that may cause problems if it is not dampened. If implemented on a three-phase system the filter will consist of three identical copies of the one illustrated in Fig. 13, one per phase.

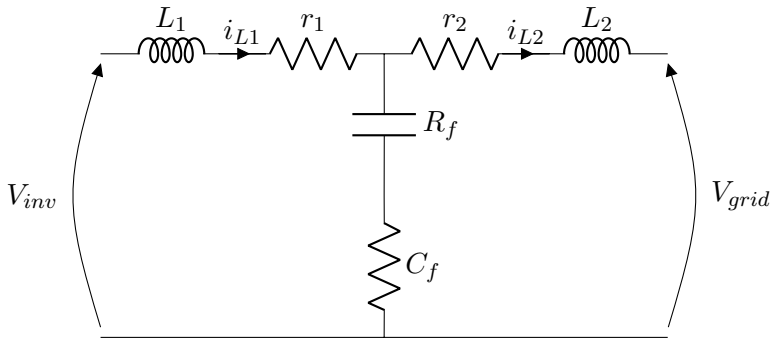

Figure 13: Circuit diagram of a single-phase LCL-filter with a damping resistor.

When designing the filter, multiple factors have to be considered such as sufficient harmonics reduction, close to unity power factor (PF) injection to the grid and filter cost minimization. The design methodology presented in [19] considers these factors when calculating the filter parameters. To limit the peak-to-peak current ripple in i_{L1}, the input-side inductor is sized according to Eq. 13.

$$L_1 = \frac{V_{DC}}{6 f_{sw}} \Delta I_{L_1 max} = \frac{V_{DC}}{6 f_{sw}} \cdot \frac{I_{ripple,\%}}{100} \cdot \frac{P_{inv}\sqrt{2}}{3 V_{inv,ph}} \tag{13}$$

$I_{L_1 max}$ denotes the maximum peak-to-peak ripple of i_{L1} in absolute terms, $I_{ripple,\%}$ denotes the same ripple, but as a percentage of the rated current and

$V_{inv,ph}$ denotes the rated phase-to-neutral voltage of the inverter. Further, to limit the power factor variation to a certain level, the capacitor is sized according to Eq. 14.

$$C_f = (1 - PF)\frac{P_{inv}}{V_{inv,LL}^2 \omega_{grid}} \tag{14}$$

PF denotes the power factor and ω_{grid} denotes the angular frequency of the grid. To attenuate the ripple of I_{L2} with a certain factor, k_a, relative to the ripple of I_{L1}, the grid-side inductor is sized according to Eq. 15.

$$L_2 = \frac{\sqrt{\frac{1}{k_a^2}} + 1}{C_f \omega_{sw}^2} \tag{15}$$

Lastly, the procedure in [19] proposes that the damping resistor should be sized as presented in Eq. 16, for the sake of avoiding resonance.

$$R_f = \frac{1}{3\sqrt{\frac{L_1 + L_2}{L_1 L_2 C_f}} C_f} \tag{16}$$

2.1.7 Step-Up Transformer

Power transformers are able to step up the voltage in an AC power system by making use of Ampere's law and Faraday's law of electromagnetic induction. A single-phase two-winding transformer, illustrated in Fig. 14, consists of two winding's wrapped around a magnetic core.

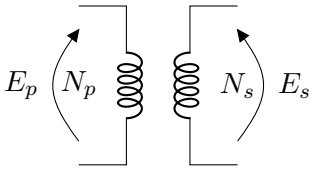

Figure 14: Ideal single-phase transformer model.

For an ideal transformer the number of turns on each side of the core determines the voltage ratio according to Eq. 17.

$$\frac{E_p}{E_s} = \frac{N_p}{N_s} \tag{17}$$

N_p and N_s are the number of turns on the primary respectively the secondary side, and E_p and E_s are the induced voltages on the primary respectively the secondary side. To more accurately represent a real transformer; winding resistances, R_p and R_s, winding leakage inductances, L_p and L_s, magnetization resistance, R_m, and magnetization inductance L_m are commonly included [20]. The equivalent electrical circuit is presented in Fig. 15.

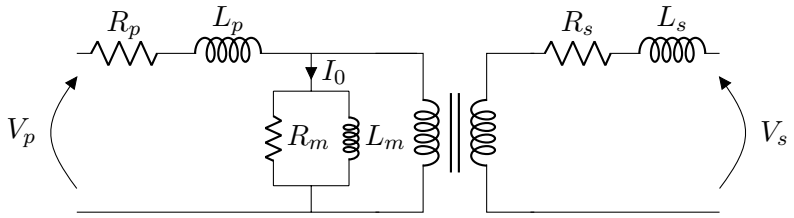

Figure 15: Circuit diagram of a non-ideal single-phase two-winding transformer.

It is possible to recalculate the secondary side impedance, Z_s, as seen from the primary side, Z'_s, according to Eq. 18.

$$Z'_s = Z_s(\frac{N_p}{N_s})^2 \tag{18}$$

Further, the magnetization impedance, Z_m, and consequently R_m and L_m can be derived from the no-load current, I_0, as presented in Eq. 19. According to [21] the no load current of a modern transformer is less than 1%.

$$\begin{aligned} Z_m &= \frac{V_p}{I_0} \\ R_m &= Z_m \cdot \frac{(1+m)}{m} \\ L_m &= Z_m \cdot (1+m) \cdot \frac{1}{2\pi 50} \end{aligned} \tag{19}$$

When extending the transformer model to its three-phase equivalent, three copies of the single phase equivalent's can be used. One extra factor to consider is the interconnection of the phases, which may or may not be the same at each side of the transformer. In a wye-conneciton the phase-to-neutral voltages are connected to one transformer winding each, while in a

delta-connection the three possible combinations of phase-to-phase voltages are connected to a one transformer winding each.

2.1.8 Distribution Cable

Conductors are needed to transport power from the PV plant to the PCC. Ideally a conductor would have zero impedance, but in reality it is not the case. Even materials with good conducting properties, such as copper and aluminium, have resistance. On top of that they will induce magnetic and electric fields when drawing current, which can be modelled with inductive and capacitive elements. A three phase cable can be represented with three PI-models with magnetic and capacitive coupling between the phases to according to Fig. 16 [22].

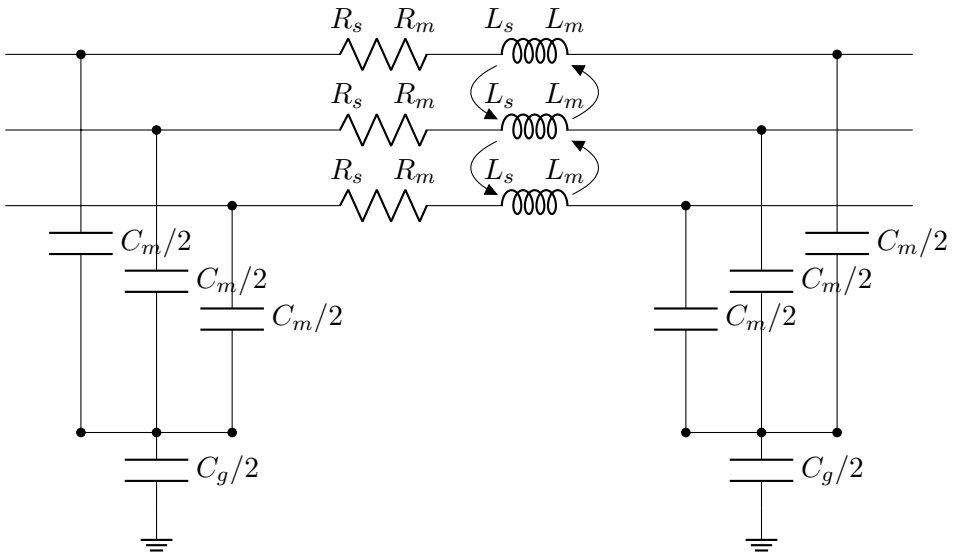

Figure 16: Circuit diagram of PI-model of a three phase cable.

C_m denotes the mutual capacitance between the phases, C_g denotes the capacitance to ground, R_m and L_m denotes the mutual- resistance and inductance the between phases, and R_s and L_s denotes the series- resistance and inductance of each phase.

2.1.9 Grid Connection

The grid properties, such as voltage level and grid strength at the PCC, need to be represented. Thevenin's theorem states that any circuit can be simplified into a voltage source in series with an impedance. Accordingly, one phase of the grid at the PCC be can modelled as in Fig. 17, where V_{grid} is a sinusoidal voltage source with the grid voltage and frequency at the PCC and Z_{grid} is an impedance that depends on the grid strength.

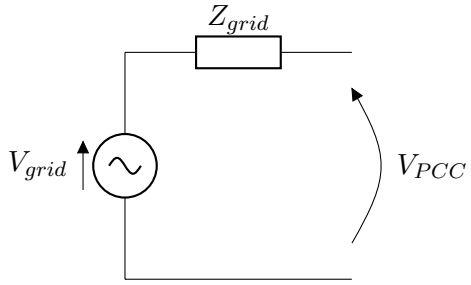

Figure 17: Circuit diagram of simplification of a single-phase grid.

The strength of the grid can be measured with the short circuit ratio (SCR) [23], defined in Eq. 20. Note that when the apparent power of the PV plant, S_{PV}, increases, the requirements on the short circuit power, S_{sc}, becomes higher for the grid to be considered equally strong. According to [24] a grid is strong if SCR > 25 and weak if SCR < 25. Further the same report mentions cases of wind farm connections at an SCR close to 2, indicating that the grid can be very weak at remote places.

$$SCR = \frac{S_{sc}}{S_{PV}} \tag{20}$$

From the short circuit power, the corresponding grid impedance can be calculated according to Eq. 21.

$$Z_{grid} = \frac{V_{grid}^2}{S_{sc}} \tag{21}$$

Combining Eq. 20 and 21 results in an expression for the grid impedance as a function of the grid strength, presented in Eq. 22.

$$Z_{grid} = \frac{V_{grid}^2}{SCR \cdot S_{PV}} \tag{22}$$

2.2 Technical Performance

In this section a selection of concepts and legislation relating to the technical performance of power generation units are introduced.

2.2.1 Stability

A very basic requirement of a grid-connected PV plant is that the electrical quantities at the PCC are stable for various inputs and disturbances. The stability criterion used in this work are:

- If all states, after some amount of time, return to their steady state value the system is asymptotically stable
- If any states diverge towards infinity, the system is unstable
- If any state stays perturbed, the system is marginally stable.

In order for the PV plant to function it is critical that all states return to their steady-state value, hence asymptotic stability is required. All elements between an input signal and an output signal contributes to the transfer function and the system's stability. The same goes for elements between a disturbance signal and the output signal. As a consequence changing filter parameters, size and number of transformers, grid strength, cable length, control loop bandwidths etc. will influence the stability of the system.

2.2.2 Time Delays

Time delays are a classical problem in control systems. In the case of utility-scale PV plants these occur when attempting to control an inductive current. Simplifying the system to the inverter output voltage, the equivalent grid voltage and an intermediate inductance as in Fig. 18 gives Eq. 23.

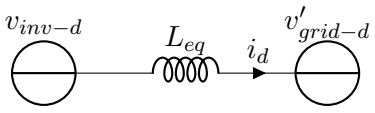

Figure 18: Circuit diagram of the current flow through an inductance.

$$\frac{di_d}{dt} = \frac{v_{inv-d} - v'_{grid-d}}{L_{eq}} \tag{23}$$

That is, there will be a delay in the current control which is proportional to the equivalent inductance between the VSI output and the PCC. In the case of utility-scale PV plants filters, cables, transformers and the grid equivalent inductance contribute to the equivalent impedance.

2.2.3 Power Quality

Power quality is a general term for the quality of quantities such as voltage, current and frequency, in an electrical system. Among others it captures how closely the AC currents and voltages resemble pure sinusoidals. It is of interest for this work, since non-linear components such as inverter-based production units create distorted current- and voltage waveforms [7]. Power quality can be quantified and measured in various ways. The measure total harmonic distortion (THD) is the euclidean norm of the amplitude of the harmonics divided by the amplitude of the fundamental signal, in short, a measure of the distortion of the sinusoidal [25].

2.2.4 Requirements for Generators

Requirements for generators (RFG) [26] is a grid code regulation introduced by the European Union in 2016 to ensure a fair, cost effective, well-functioning and reliable electricity market in the union. The regulation requires the generator modules to fulfill certain technical performance criteria and robustness requirements to connect to the grid. In order to achieve a reliable system, the regulation regulates how generator modules are supposed to respond when the system conditions differs from normal operating conditions, such a voltage and frequency deviations. In the regulations, generators are divided into different categories depending on their rated capacity and/or PCC voltage level, whether they are synchronous or not and whether they are offshore or not. Large-Scale PV plants (>30 MW) belongs to the category Power Park Modules (PPMs) of type D. Some requirements applicable for type D PPMs are that they should be able to:

- Stay connected and work at 47.5-51.5 Hz for at least 30 minutes [26].
- Stay connected and work at frequency rate of changes of 2 Hz/s [27].
- Supply constant active power, equal to reference value, independent of frequency changes [26].

The regulation is extensive and many aspects will not be treated for various reasons.

3 Methodology

In this chapter the methodology used to achieve the research goals is presented.

For the first research goal simulations were carried out on two different models, with different numbers of transformers, under sets of conditions that the system might be exposed to. In short: how the behaviour of the two systems would differ in operation. During these the behaviour was analysed through measuring select magnitudes in the simulation model. This will be refereed to as general performance test and is described in Sec. 3.1.

For the second research goal simulations were carried out on four models where one key parameter was changed until the system was no longer asymptotically stable, to get a quantitative measure on each model's robustness. This will be refereed to as stress test and is described in Sec. 3.2.

For the third research goal a review of literature was combined with consultation of people in industry. Since this is quite different from the other goals, this procedure will be presented in Ch. 6.

The validity of the results of a simulation are only as good as the model on which they were run. For this reason a large amount of this work was spent on building accurate simulation models for the simulations. This work is presented in Sec. 3.3. Four models were built, representing a 40 MW utility-scale PV plant with 4 x 10 MVA transformers (model A), 20 x 2 MVA transformers (model B), 1 x 40 MVA transformers (model C) and 40 x 1 MVA transformers (model D). Model A and B were used both for the general performance test and the stress test, while the model C and D were only used for the stress test. These two were introduced to represent extreme cases in order to get more pronounced differences between the models, rather than representing realistic scenarios, and were not included from the beginning. Hence, they were not used for the general performance test.

3.1 General Performance Test

In order to test and compare the models under varying conditions, cases covering combinations of site parameters with external disturbances were formulated.

Site Parameters

The site parameters that were varied were grid strength, cable length between internal transformers and PCC and the transformer inductances. All these parameters affect the equivalent inductance between the VSI and PCC which, as stated in Sec. 2.2.2, affects the time delay in the current control. Hence, it was regarded interesting to examine if any combination of these parameters would cause problems for any of the models.

The grid strength was categorized as weak/strong, where strong was an SCR of 25, in accordance with Sec. 2.1.9. It was desired that the weak grid was significantly weaker than the strong grid, for this reason an SCR of 3 was chosen. Note that this value is in compliance with Sec. 2.1.9.

The cable length was divided into short/long as 1/10 km. The cable length between internal transformers and PCC varies from project to project and since detailed schematics of PV plants are hard to come by, these values were rough estimations. It could also be that the internal transformers are geographically spread out in the plant and therefore at different distances to the PCC. It was suspected that such a situation, with asymmetric cable lengths, potentially would cause problems. Hence, a simulation case was added wherein a quarter of the cables were long (10 km) and the rest were short (1 km). A factor 10 in difference in cable length, while not particularly realistic according to [28], was chosen as it would clearly show if an asymmetric cable length affects the different models in the same way or not.

Further, according to [28] the leakage inductance of transformers varies between different units ordered to the same specifications. A situation with asymmetric transformer inductances was also suspected to potentially cause problems and was therefore implemented. For the four-transformer model (model A) the inductance was set in steps of 5% from 110% to 90% of the nominal inductance. For the twenty-transformer model (model B) the inductance was set in steps of 1% from 110% to 90 % of nominal inductance, skipping 100%.

External Disturbances

The external disturbances introduced were variations of the solar irradiation and a ramp in the grid frequency. The irradiation variation was set up such that the whole PV plant was exposed to the same irradiation of 1000 W/m^2 from the start, and after a while (0.2 s) the irradiation for half of the PV modules was reduced to 10% of that. This disturbance aimed to mimic the effect of a cloud shading half of the PV plant. The irradiation change occurs in a step rather than a ramp to emulate the worst-case scenario where the cloud appears from nowhere.

Large deviations in grid frequency can occur when large power producers or consumers unintentionally disconnect. To portray such a scenario, a case where the frequency of the grid was ramped up from the nominal frequency, with a rate of 2 Hz/s, until it reached 51.5 Hz, was introduced. The rate of change and maximum frequency were obtained from the RFG limits presented in Sec. 2.2.4.

Test Cases

The test cases decided on are listed in Tab. 1 and Tab. 2. The models were only subjected to one disturbance at a time and the cases with asymmetric site parameters were only tested with one disturbance, change in solar irradiation.

Table 1: Simulation cases for the general performance test of model A.

Sim. Case	**Trafo. Setup**	**Grid Strength**	**Cable length**	Z_{trafo}	**Disturbance**
A:1.1	4 x 10 MVA	Strong	Short	Nom.	Irradiation
A:1.2	4 x 10 MVA	Strong	Long	Nom.	Irradiation
A:1.3	4 x 10 MVA	Weak	Short	Nom.	Irradiation
A:1.4	4 x 10 MVA	Weak	Long	Nom.	Irradiation
A:1.5	4 x 10 MVA	Weak	Asym.	Nom.	Irradiation
A:1.6	4 x 10 MVA	Weak	Long	Asym.	Irradiation
A:1.7	4 x 10 MVA	Strong	Short	Nom.	Grid Freq. Ramp
A:1.8	4 x 10 MVA	Strong	Long	Nom.	Grid Freq. Ramp
A:1.9	4 x 10 MVA	Weak	Short	Nom.	Grid Freq. Ramp
A:1.10	4 x 10 MVA	Weak	Long	Nom.	Grid Freq. Ramp

Table 2: Simulation cases for the general performance test of model B.

Sim. Case	**Trafo. Setup**	**Grid Strength**	**Cable length**	L_{trafo}	**Disturbance**
B:1.1	20 x 2 MVA	Strong	Short	Nom.	Irradiation
B:1.2	20 x 2 MVA	Strong	Long	Nom.	Irradiation
B:1.3	20 x 2 MVA	Weak	Short	Nom.	Irradiation
B:1.4	20 x 2 MVA	Weak	Long	Nom.	Irradiation
B:1.5	20 x 2 MVA	Weak	Asym.	Nom.	Irradiation
B:1.6	20 x 2 MVA	Weak	Long	Asym.	Irradiation
B:1.7	20 x 2 MVA	Strong	Short	Nom.	Grid Freq. Ramp
B:1.8	20 x 2 MVA	Strong	Long	Nom.	Grid Freq. Ramp
B:1.9	20 x 2 MVA	Weak	Short	Nom.	Grid Freq. Ramp
B:1.10	20 x 2 MVA	Weak	Long	Nom.	Grid Freq. Ramp

The parameters measured to analyse the behaviour were:

- V_{PCC} - Phase voltages at the PCC.
- THD of V_{PCC} - THD of the phase voltages at the PCC.
- V_{DC} - DC-link capacitor voltage (measured at two different branches).
- i_{d-inv} & $i_{d-inv-ref}$ - Inverter direct-component current & its reference value (measured at two different branches).
- i_{branch} - Current injected to the PCC from one transformer branch (measured at two different branches).
- P_{grid} - Grid injected active power.

V_{PCC} was perhaps the most obvious parameter to measure. Its distortion is regulated by IEEE standard 519-2022 [29] and problems within the plant which affect the grid would be visible here. The THD of the PCC voltage quantifies how it diverges from a 50 Hz sinusoidal. It was calculated using MATLAB Simulink's built in *THD* block. V_{DC} and i_{d-inv} were chosen since the outer control loop for the VSI controls the former, while the inner control loop for the VSI controls the later and these controllers being able to follow their references is crucial for the performance of the plant. For i_{d-inv} the set-point varies and is thus measured so as to see if i_{d-inv} follows it. This

is not needed for V_{DC}, since its reference is a fixed value. i_{branch} is the current measured at the output of one branch. It was measured to see if any resonance occurs between branches. V_{DC}, i_{d-inv} and $i_{d-inv-ref}$ were only measured for one branch, since doing measurements slowed down the simulation speed. For the same reason i_{branch} was only measured for two branches, the minimum number that could give any indication of resonance between branches. P_{grid} is important for two reasons; the efficiency and the RFG requirement stating that PPMs should inject constant active power. The efficiency is only interesting to compare between the models in steady state. For this reason it was deemed enough to compare in cases A/B:1.1 and A/B:1.2.

3.2 Stress Test

To find how the robustness of the system depends on the size and number of transformers, four models were built with 1, 4, 20 and 40 transformers. Each model was run with a decreasing grid strength until the system was no longer asymptotically stable. Adjusting the grid strength, and not some other parameter, was decided on because it was found in the general performance test that it was the parameter with greatest impact on the system robustness, and therefore an appropriate way to stress the system. The grid strength was decreased by reducing the SCR, and thus increasing the grid impedance, in steps of 0.05. In this way the minimum grid strength, measured in SCR, was found within a range of 0.05. The minimum tolerable grid strength for the different models were then compared. For these tests long cables were used and an irradiation variation was applied as described in Sec. 3.1. These conditions were chosen as they, in the previous test, would stress the system the most.

Early on in testing, it was found that when lowering the SCR there is a breaking point at which the system behaviour changes wildly. Going from being well-behaved to collapsing. This point coincides with the controllers no longer being able to follow their reference and the system no longer being asymptotically stable. This point was used as the metric of failure for the stress test. This phenomenon will be termed control failure for easier reference. The stress test cases are presented in Tab. 3.

Table 3: Simulation cases for the stress test.

Sim. Case	**Trafo. Setup.**	**Cable length**	**Disturbance**
A:2	4 x 10 MVA	Long	Irradiation
B:2	20 x 2 MVA	Long	Irradiation
C:2	1 x 40 MVA	Long	Irradiation
D:2	40 x 1 MVA	Long	Irradiation

3.3 MATLAB Simulink Model

The four simulation models were built in MATLAB Simulink utilizing the Simscape Electrical - Specialized Power Systems extension. The systems were composed of a number of subsystems which they shared. Branches consisting of PV arrays, power electronic converters and filters were the base. For all models, 40 of these were used with a power of 1 MW each. These were then connected via transformers and cables to a grid model, from which the phase angle was tracked with a PLL algorithm. The differences between the models are different numbers of transformers and corresponding adjustments such as different cables and controller settings.

3.3.1 Implementation of a Branch

As mentioned above four different models were built, but they all shared many components. To begin with, a branch was built consisting of PV modules, power electronic converters and filters. This branch was then used as a base for all four models. This section describes how one such branch was implemented. It includes which blocks were used and how these were connected to represent hardware and implement functionalities. It also describes the method used to set parameter values.

PV Array

The PV arrays were implemented with *PV Array* blocks. A module with following properties was arbitrarily chosen; $P_{MPP} = 290\ W$ and $V_{MPP} = 31.7\ V$. The number of PV modules per string and the number of PV strings in parallel were set according to two conditions; each PV array should generate approximately 1 MW power and the output voltage should be above the DC-link voltage, since the buck converter which follows the PV arrays can not raise the voltage for the DC-link capacitor. To fulfill both criteria, an appropriate setup was 77 modules per string and 45 parallel strings. Fig. 19 illustrates the implementation. It consists of no more than the *PV*

Array block which takes a step as input in the irradiation and a constant cell temperature, *temp*. It has a positive and a negative output, +, -, and a output for measurement values, m.

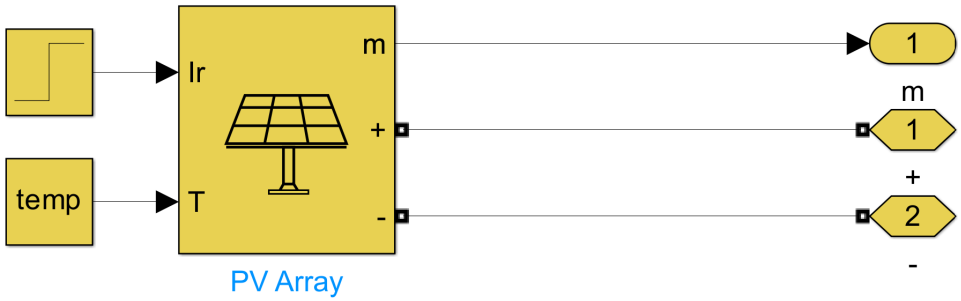

Figure 19: PV array - Simulink implementation.

Buck Converter and MPPT

The DC-DC buck converter was implemented as a *Buck Converter* with a capacitor on the input set according to Eq. 4 along with a filtering inductor on the output set according to Eq. 3, where a ΔI of 20 % of the maximum power point current was used. The buck converter is then controlled with firing pulses from a PWM. The value of f_{sw} was chosen to 10 kHz, which is within the scope of what is common for the application. The exact value is not of great concern in a comparative analysis, since it will effect all the models in the same manner. The reference for the PWM is, in turn, generated by a discrete implementation of the P&O MPPT algorithm as described in Sec. 2.1.3 operating on measurements from the aforementioned PV-array. The sampling time and perturbation size were set experimentally. Fig. 20 illustrates the implementation.

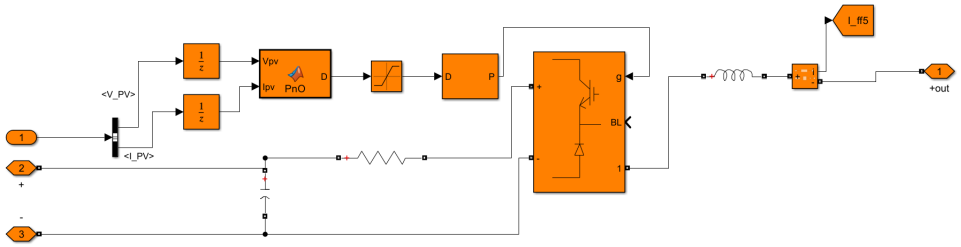

Figure 20: Buck converter - Simulink implementation.

VSI

The DC-AC converter / VSI was implemented as a *Two-level Converter*. At the input of the the VSI a DC link capacitor, C_{DC}, was placed. It was designed as stated in Eq. 6 to attain a maximal voltage ripple of 3%. As with the DC-DC converter the exact switching frequency, f_{sw}, was not considered particularly important and was chosen within what is common for the application to the same value as for the buck converter. No method was found in literature for setting V_{DC} and it was instead set experimentally. The values chosen for f_{sw} and V_{DC} are presented in Tab. 4.

Table 4: VSI related parameters.

Parameter	**Rating**
V_{DC}	$1500\,V$
f_{sw}	$10\,kHz$

The VSI was controlled in accordance with the theory presented in Sec. 2.1.5, hence, the following four PI-controllers had to be tuned:

PI_1 - Control of I_d current

PI_2 - Control of I_q current

PI_3 - Control of DC link voltage

PI_4 - Control of grid injected reactive power

PI_3 generates a reference to PI_1, while PI_4 generates a reference to PI_2, in other words there are two outer-inner loop pairs. The parameters of PI_1 and PI_2 were tuned in a theoretical manner by combining the rules of thumb with the equations presented in Sec. 2.1.5, resulting in the expressions in Eq. 24.

$$\begin{aligned} P &= \frac{1}{\lambda} \cdot L_{eq} = \frac{2\pi f_{sw}}{10} \cdot (L_1 + L_2 + n_1 \cdot (L_p + L'_s) + n_2 \cdot L'_{cable}) \\ I &= \frac{1}{\lambda} \cdot R_{eq} = \frac{2\pi f_{sw}}{10} \cdot (r_1 + r_2 + n_1 \cdot (R_p + R'_s) + n_2 \cdot R'_{cable}) \end{aligned} \tag{24}$$

As seen in Eq. 24, factors n_1 and n_2 have been included. These were included to compensate for an additional voltage drop when connecting branches radially. Consider Fig. 21; the additional currents through $Z_{transformer}$ and Z_{cable} will cause an increased voltage drop by a factor of the number of VSI

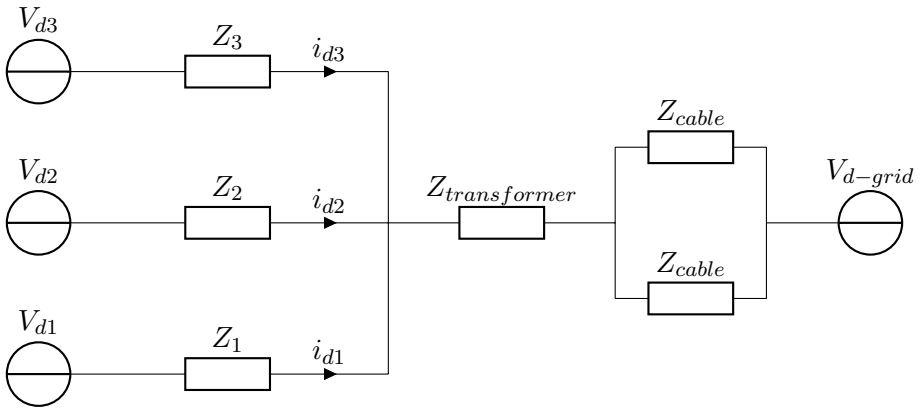

Figure 21: Circuit diagram illustrating a general case of radially connected VSIs via a transformer and cables to the grid.

branches supplying current through the impedance. In the case of Fig. 21, $n_1 = 3$ and $n_2 = 3/2$.

The proportional part of PI_3 is expressed in Eq. 25 and was, as stated in Sec. 2.1.5, related to the dynamics of C_{DC} and the desirable bandwidth. However the integrator part, I, was tuned experimentally and was raised until the steady state error of the step response approached zero fast, while still maintaining a closed loop bandwidth in accordance with the rules of thumb in Sec. 2.1.5. The bandwidth was estimated by setting up a simplified closed loop transfer function of the DC voltage dynamics where the inner control loop and the switching dynamics where set to one, a simplification on account of them being much faster. Lastly, the parameters of PI_4 were tuned entirely in a experimental manner. The goal of this controller was to affect the PCC voltage as little as possible. After some tweaking an equilibrium was found where the PCC voltage settled at rated level reasonably quick, while not affecting the robustness of the system too much. The exact setting of the controllers are presented in App. A. Fig. 22 shows the implementation of the VSI and its controllers.

$$P = \frac{1}{\lambda} \cdot C_{DC} = \frac{2\pi f_{sw}}{100} \cdot \frac{V_{DC}}{V_{inv}} \cdot C_{DC} \tag{25}$$

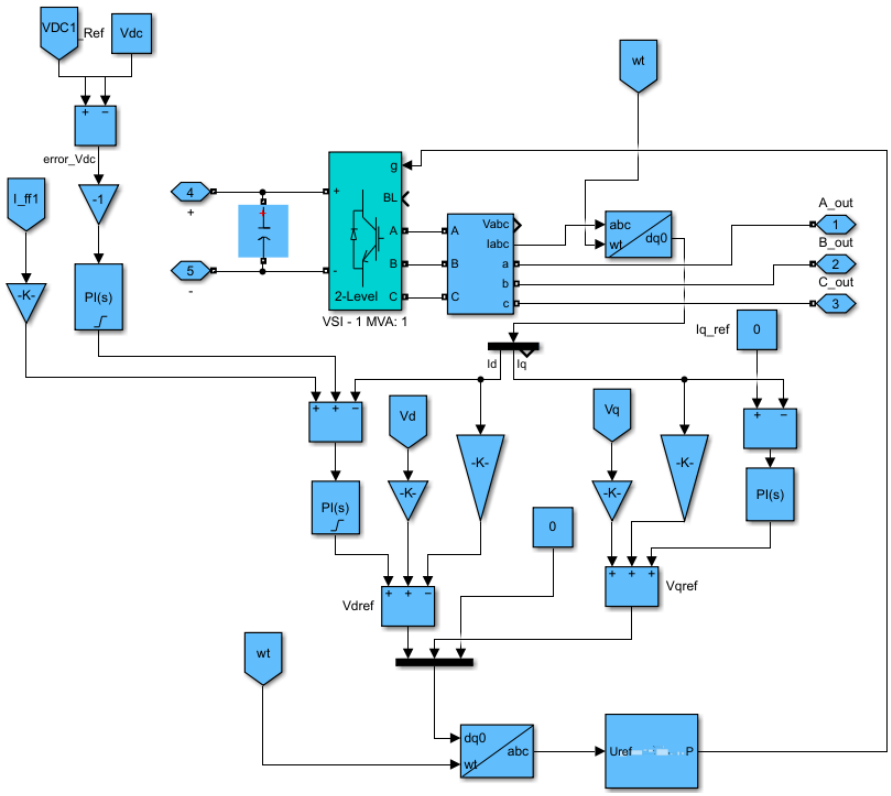

Figure 22: VSI - Simulink implementation.

Internal cables, between the different components in one branch, were omitted from the model for a number of reasons. Being short their impact would be negligible in comparison to the passive components, while including them would mean more work in building the model and make the simulations heavier. In addition it would be hard to estimate their length as it is very dependent on the specific plant.

LCL-filter

The LCL-filter was sized according to Eqs. 13, 14, 15 and 16 with the following design considerations:

- Maximum current ripple in I_{L1}: 10 %
- Maximum power factor variation: 5 %
- Attenuation from I_{L1} to I_{L2}: 20 %

These considerations resulted in a filter output current with a peak-to-peak ripple of 2 %. When building a simulation model the cost of the filter may not seem important, but in order to simulate a realistic PV system these considerations were regarded as a reasonable trade-off between cost and harmonics attenuation. Fig. 23 shows the LCL-filter implementation.

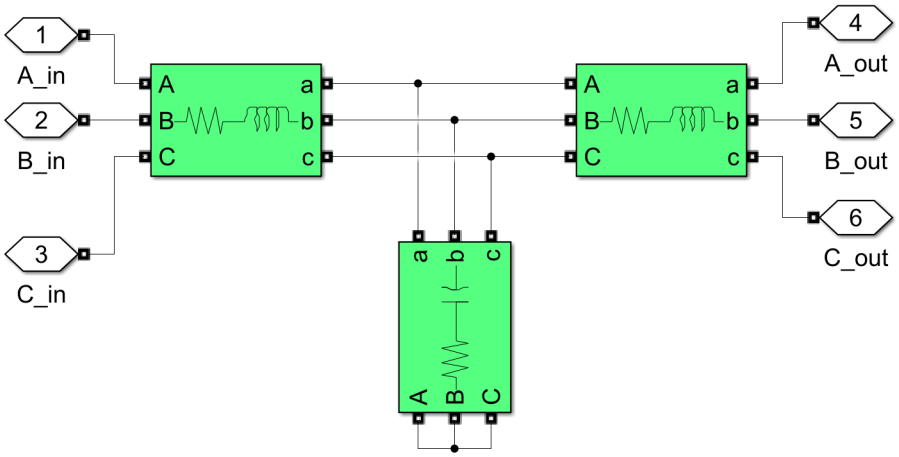

Figure 23: LCL-filter - Simulink implementation.

PLL

The PLL algorithm was implemented using the *PLL (3ph)* block, which was fed with the three phase to ground voltages at the PCC. Fig. 24 illustrates the implementation. Note that it is not part of the branch, instead each model makes use of one common PLL algorithm at the PCC.

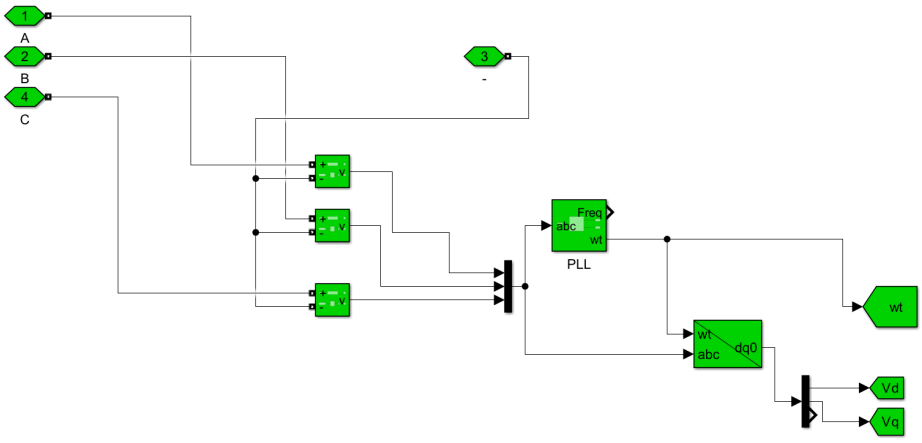

Figure 24: PLL algorithm - Simulink implementation.

3.3.2 Model Variations

With what is described in 3.3.1 four models were built with 1, 4, 20 and 40 internal transformers. Altering the transformer setups also implied changes to the controllers, since it changes the impedance that each inverter sees.

Fig. 25 illustrates the implementation of the four-transformer model (model A). In the illustration, the branches connected to all but one of the transformers were omitted to make the model easy to survey. Note that branches were connected to the three bottom transformers in the way here illustrated for the top transformer.

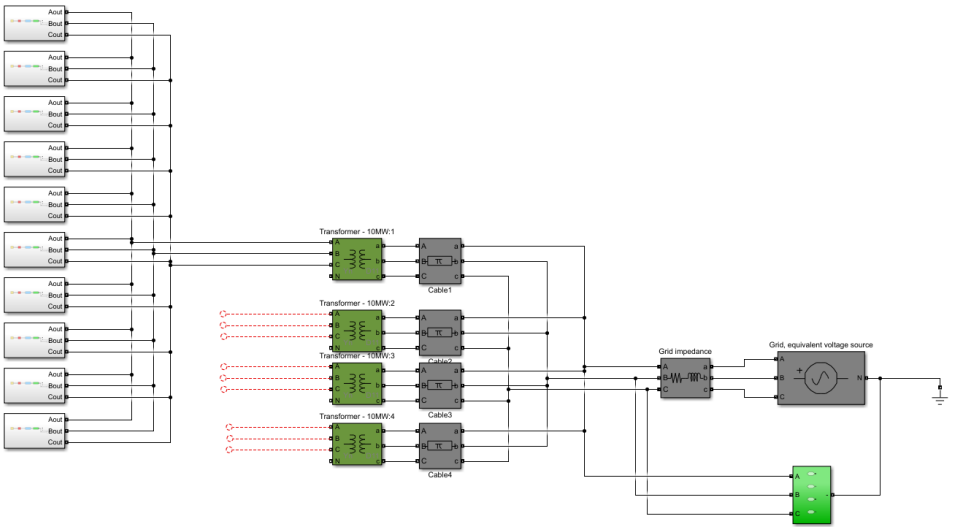

Figure 25: The implementation of simulation model A.

As mentioned earlier in this section, each of the four models makes use of 40 branches. Simulation model A has, as seen in Fig. 25, 10 branches connected to each transformer and each transformer is connected via one cable to the PCC. Simulation model B has two branches connected to each transformer and each transformer is connected via one cable to the PCC. Simulation model C has 40 branches connected to a single transformer which is in turn connected via four cables to the PCC. Simulation case D has one branch connected to each transformer and pairs of transformers are connected via one cable to the PCC. That is, two transformers share one cable for this case.

The transformers were implemented as *Three-Phase Transformers (Two Windings)* with wye (Yn) connections at the converter side and delta (D11) connections at the grid side, which are the industry standard connections for transformers in this application area [28]. The no-load current of the transformers was estimated to one percent of the rated current and the X/R-ratio of the magnetizing branch was estimated to ten, independent of transformer rating. Consequently, the magnetizing resistance and inductance were calculated according to Eq. 19. Datasheets [30, 31, 32, 33] of well-known transformer manufacturers provided leakage impedance values for the different transformer ratings, presented in Tab. 5. Half of the total per-unit leakage impedance was set to each side of the transformer. The X/R ratio was set to 20 for all transformers, a common value for transformers with rated capacity's of this order of magnitude[34].

Table 5: Leakage impedance values for different transformers.

Trafo. Rating.	$Z_{leakage}$ [%]
1 MVA	5.7
2 MVA	6.4
10 MVA	7.62
40 MVA	12.5

The subsequent cables, connecting the transformers with the PCC, were modeled as *Three-Phase PI Section Lines*. It takes resistance, inductance and shunt capacitance as inputs. The values used were gathered from a datasheet from a well-known cable manufacturer [35]. Depending on the number of transformers, the number of cables and the current through them differs. For this reason cables of different thickness were used for different models. A decision was made that underground cables, and not overhead power lines, would be considered because it is the standard nowadays [28]. The two models with the fewest amount of transformers were connected to the PCC with four cables, while the other two models were connected with twenty cables. The cable data that was used is presented in Tab. 6.

Table 6: Cable parameters.

Cable Setup	**Cable**	**Current capacity [A]**	R [Ω / km]	L [mH / km]	C [μ F / km]
4 x 10 MVA	3x240/25AI	340	0.125	0.3	0.27
20 x 2 MVA	3x25/25AI	100	1.2	0.13	0.43

4 Results

In this chapter the results of the two tests, the general performance test and the stress test, used to gauge the difference in technical performance between the models are presented. In this chapter the behaviour will only be described and not discussed until Ch. 5. Sec. 4.1 deals with the general performance test while Sec. 4.2 deals with the stress test. The figures in this chapter will be presented side by side for ease of comparison. This has the unfortunate drawback of making it harder to distinguish details. Still it was considered preferable to do it this way and those who wish to have a closer look are refereed to using the PDF version and zooming.

4.1 General Performance Test

The general performance test consisted of the simulation cases listed in Tab. 1 and Tab. 2. A sample of plots of the parameters measured from these will be presented here. The long cable cases were found to give more interesting results than their short cable counterparts. For this reason, and to limit how much is presented in this section, the short cable cases will be presented in App. B. Tab. 7 summarizes the simulation cases and where their results are presented.

Table 7: Summary of the simulation cases in the general performance test

Sim. Case	**Description**	**Results illustrated in**
1.1	Strong grid, short cables, irr.	Appendix
1.2	Strong grid, long cables, irr.	Results
1.3	Weak grid, short cables, irr.	Appendix
1.4	Weak grid, long cables, irr.	Results
1.5	Asymmetric cable lengths	Appendix
1.6	Asymmetric transformer inductances	Results
1.7	Strong grid, short cables, freq.	Appendix
1.8	Strong grid, long cables, freq.	Results
1.9	Weak grid, short cables, freq.	Appendix
1.10	Weak grid, long cables, freq.	Results

4.1.1 Variation of Solar Irradiation

Case 1.2

To begin with, the cases A:1.2 and B:1.2 (strong grid, long cables and irradiation variation), are compared. These cases will be used as base cases. A few different quantities chosen to compare the technical performance in terms of stability, power quality and efficiency are presented in Figs. 26-29.

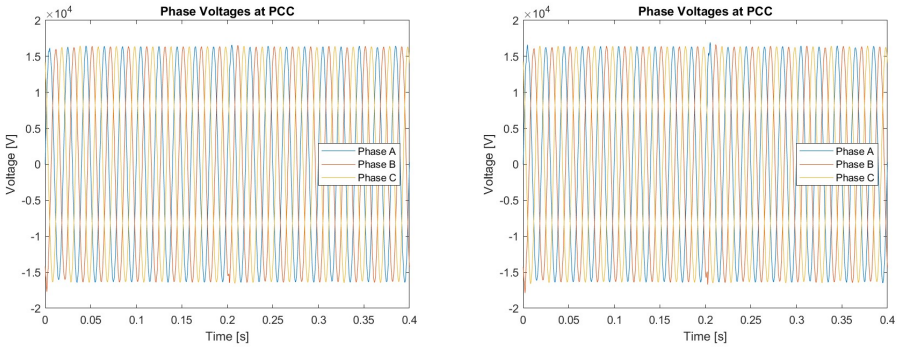

(a) A:1.2. (b) B:1.2.

Figure 26: Phase voltages at PCC in simulation cases A:1.2 & B:1.2.

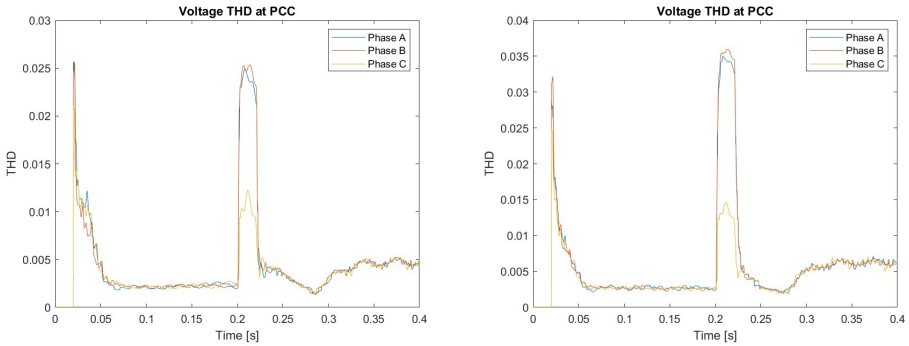

(a) A:1.2. (b) B:1.2.

Figure 27: Voltage THD at PCC in simulation cases A:1.2 & B:1.2.

Figure 26 displays the phase voltage waveforms at the PCC, where both models show a steady behaviour with high power quality through the whole simulation. This is further indicated by the PCC voltage THD, presented in Fig. 27, which is close to zero ($\approx 0.5\%$) in steady state for both models. At the beginning and at the moment of solar irradiation change (0.2s) the THD spikes for both models, these are a bit higher for the 20x2 MVA transformer model, ≈ 0.01. The DC link voltage is plotted in Fig. 28 and is close to identical and within 0.4 % from the reference value, for both models. This

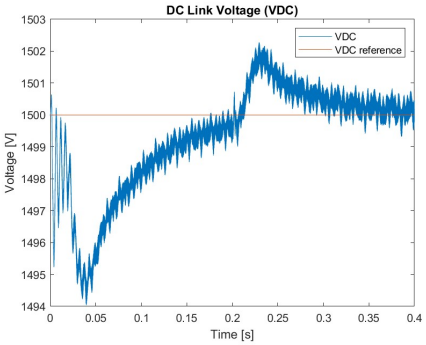

(a) A:1.2.

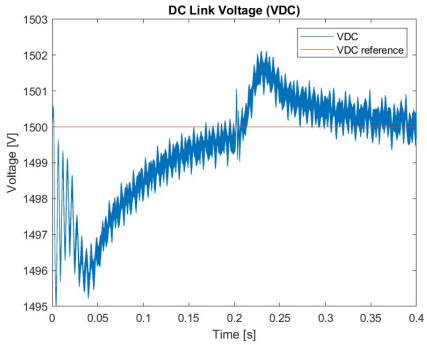

(b) B:1.2.

Figure 28: DC link voltage in simulation cases A:1.2 & B:1.2.

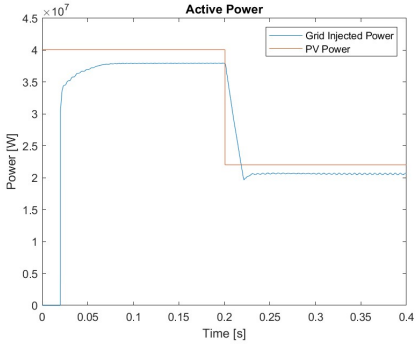

(a) A:1.2.

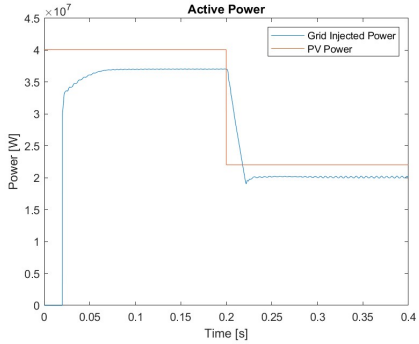

(b) B:1.2.

Figure 29: Active power in simulation cases A:1.2 & B:1.2.

is a small deviation as it was designed for voltage deviations of up to 3 %. This indicates that both control systems easily manages to deal with the disturbance. The active power injected at the PCC from the PV system is plotted in Fig. 29 along with the power generated from the PV modules. The behaviour for the two models is very similar. In Tab. 8 the system efficiency in steady state, calculated with the average grid injected power from t = 0.1 to t = 0.2, is presented for the base cases case 1.1 and case 1.2. It is very similar for the two models in case 1:1, but there is a difference of around 2.3 percentage points in case 1:2.

Table 8: Steady state system efficiency for cases case 1.1 and case 1.2.

Case	**System Efficiency** [%]	
	Model A	Model B
1.1	97.07	97.04
1.2	94.68	92.39

Case 1.4

Presented in Figs. 30-33 are comparisons between the cases A:1.4 and B:1.4 (weak grid, long cables and irradiation variation).

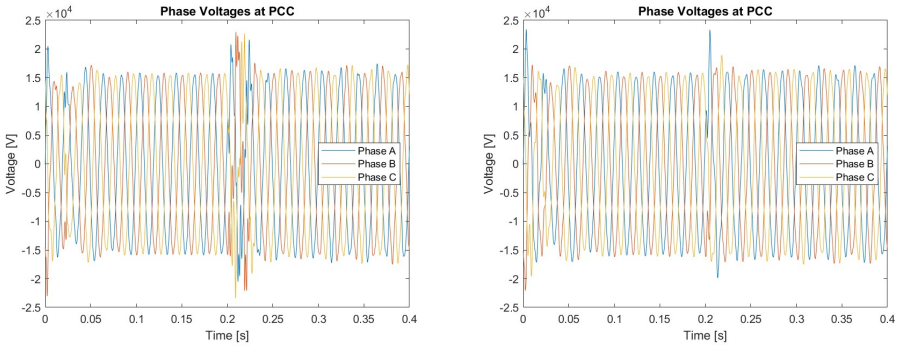

(a) A:1.4. (b) B:1.4.

Figure 30: Phase voltages at PCC in simulation cases A:1.4 & B:1.4.

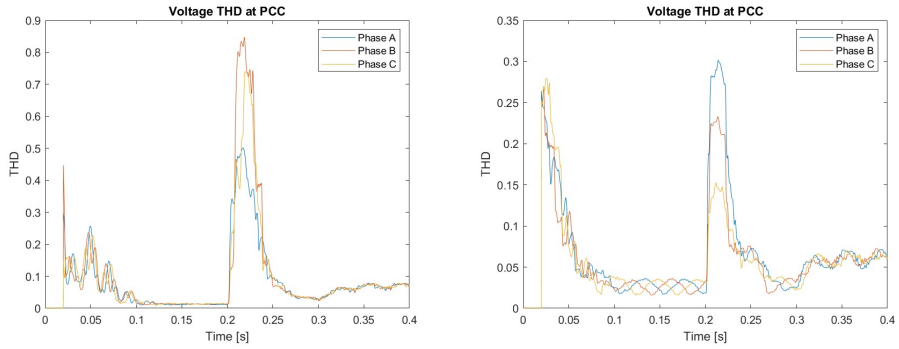

(a) A:1.4. (b) B:1.4.

Figure 31: Voltage THD at PCC in simulation cases A:1.4 & B:1.4.

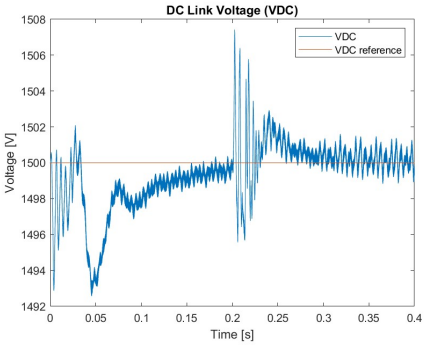

(a) A:1.4.

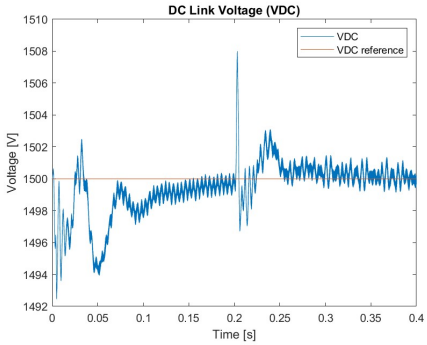

(b) B:1.4.

Figure 32: DC link voltage in simulation cases A:1.4 & B:1.4.

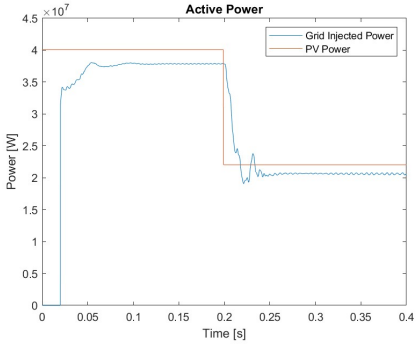

(a) A:1.4

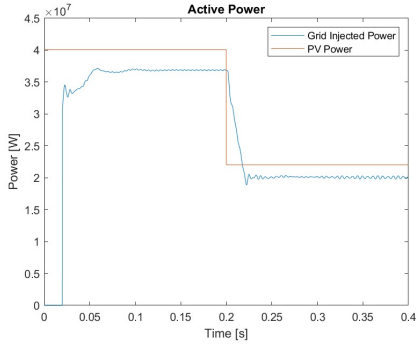

(b) B:1.4.

Figure 33: Active power in simulation cases A:1.4 & B:1.4.

Fig. 30 displays the phase voltage waveforms at the PCC, which are no longer as steady and clean as in the base case. Distortion appears at the start of the simulation and at the change of irradiation. The distortion is more severe for model A than model B. This difference in distortion is quantified in Fig. 31. A difference in DC link voltage is also visible in Fig. 32 but the controller manages to follow the reference in both cases. Fig. 33 shows a slight disturbance in the active power and a slight difference in the active power in the two cases.

4.1.2 Asymmetrical

Case 1.6

Simulation cases A:1.6 and B:1.6, which corresponds to weak grid, long cables and asymmetrically perturbed transformer inductance with varying solar irradiation, are presented in Fig. 34-37. Simulation cases A:1.5 and B:1.5, corresponding to weak grid, asymmetrically perturbed cables showed little difference in behaviour between models and the phenomenon observed were more clear in A:1.6 and B:1.6. For this reason they will be omitted from the results chapter.

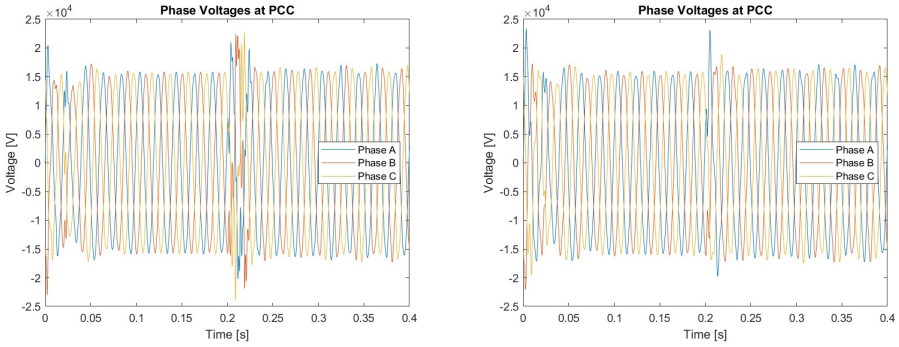

(a) A:1.6. (b) B:1.6.

Figure 34: Phase voltages at PCC in simulation cases A:1.6 & B:1.6.

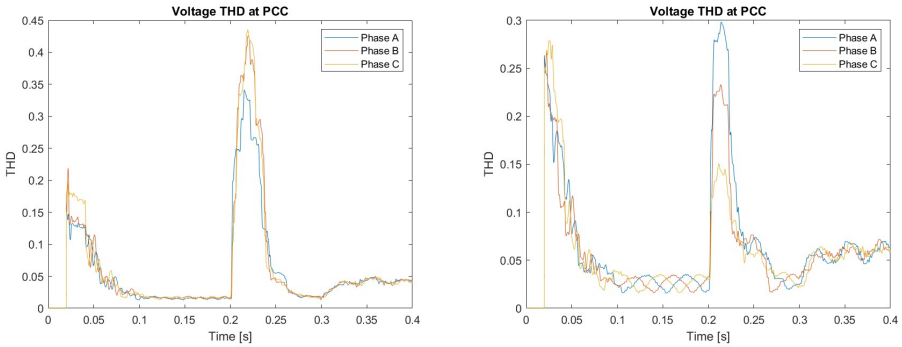

(a) A:1.6. (b) B:1.6.

Figure 35: Voltage THD at PCC in simulation cases A:1.6 & B:1.6.

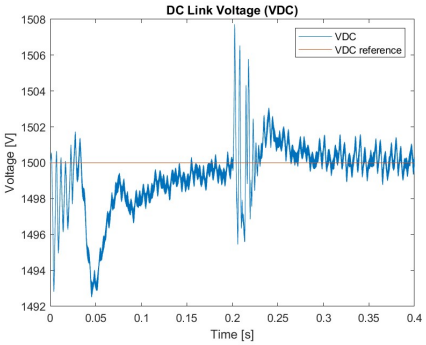

(a) A:1.6.

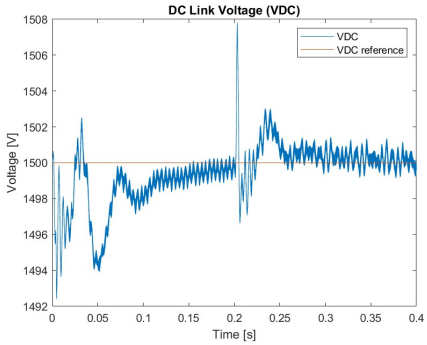

(b) B:1.6.

Figure 36: DC link voltage in simulation cases A:1.6 & B:1.6.

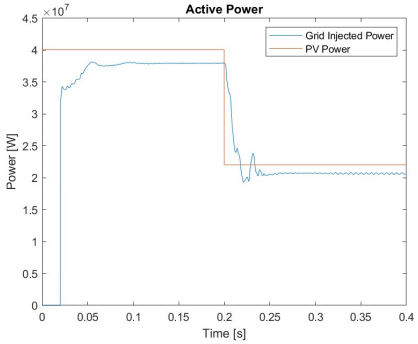

(a) A:1.6.

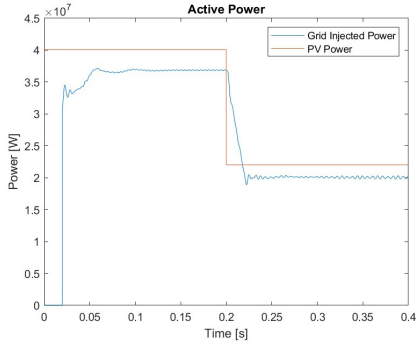

(b) B:1.6.

Figure 37: Active power in simulation cases A:1.6 & B:1.6.

Fig. 34 shows the phase voltages in the PCC. For both models these are disturbed at the simulation start and at the change of solar irradiation being more severe for the 4 transformer model. This is also visible in Fig. 35. The DC link voltage once again manages to follow its reference closely but is perturbed at the same points in time as the PCC voltage as seen in Fig. 36. The behaviour differs slightly between models. Fig. 37 shows an active power which stabilizes fairly quickly for both models after being disturbed. Once again there is a difference in behaviour between models with model A looking slightly worse.

4.1.3 Grid Frequency Ramp

Case 1.8

Simulation cases A:1.8 and B:1.8, which corresponds to strong grid, long cables and a grid frequency ramp as disturbance, are presented in Fig. 38-41.

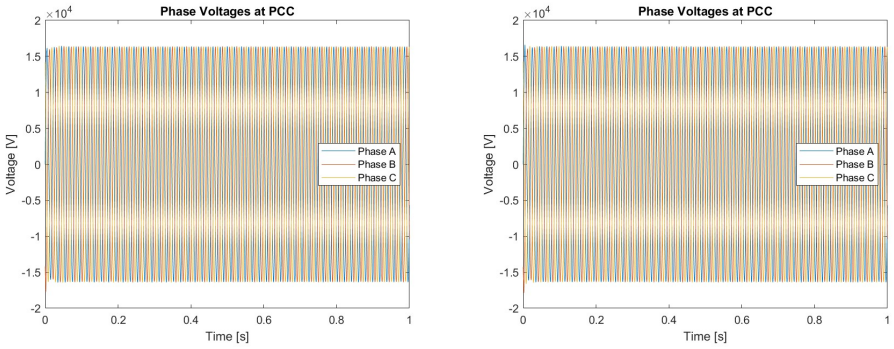

(a) A:1.8. (b) B:1.8.

Figure 38: Phase voltages at PCC in simulation cases A:1.8 & B:1.8.

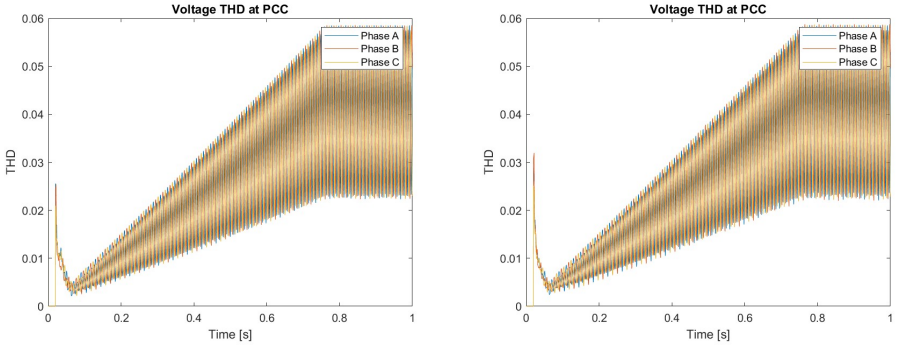

(a) A:1.8. (b) B:1.8.

Figure 39: Voltage THD at PCC in simulation cases A:1.8 & B:1.8.

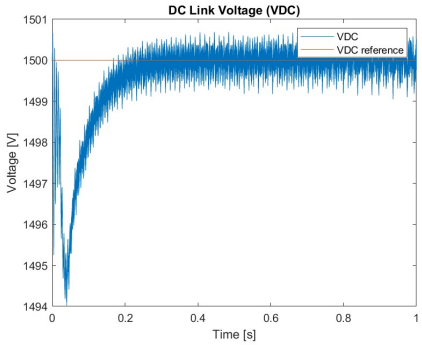

(a) A:1.8.

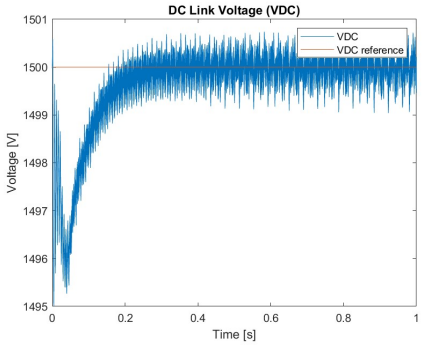

(b) B:1.8.

Figure 40: DC link voltage in simulation cases A:1.8 & B:1.8.

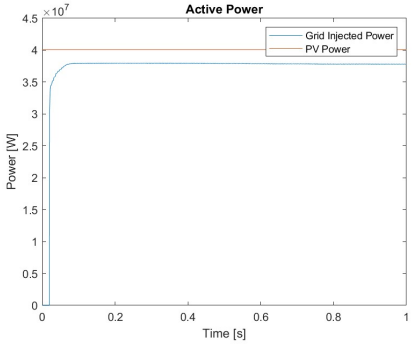

(a) A:1.8.

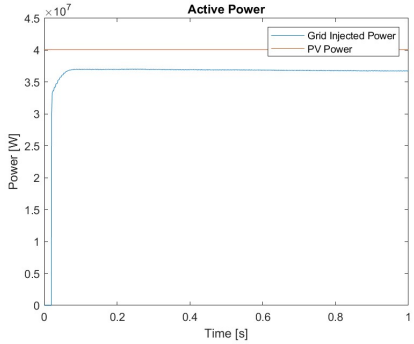

(b) B:1.8.

Figure 41: Active power in simulation cases A:1.8 & B:1.8.

The PCC voltage waveforms are displayed in Fig. 38 and stay at nominal level for both models throughout the whole simulation. The voltage THD is plotted in Fig. 39 and is identical for both models, but it is very different from the previous cases. The THD ramps along with the grid frequency, this is a measurement error which will be explained in Ch. 5. The DC link voltage is plotted in Fig. 40 and deviates with less than 0.4% from the reference value. The active power output, presented in Fig. 41, is constant through the whole simulation. There is no visible difference between the two models.

Case 1:10

Simulation cases A:1.10 and B:1.10, which correspond to weak grid, long cables and a grid frequency ramp as disturbance, are presented in Fig. 42-45

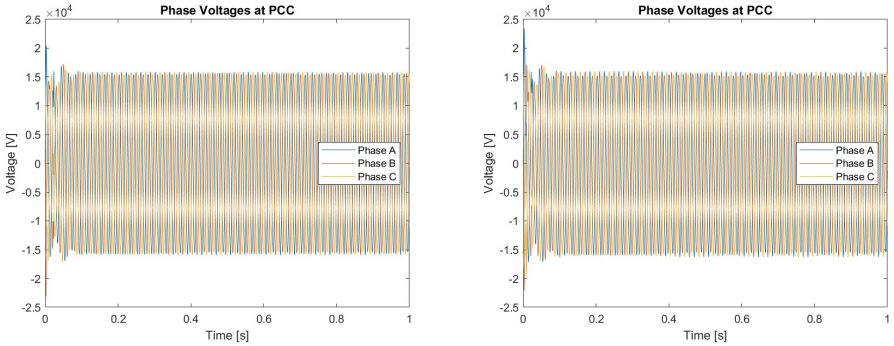

(a) A:1.10. (b) B:1.10.

Figure 42: Phase voltages at PCC in simulation cases A:1.10 & B:1.10.

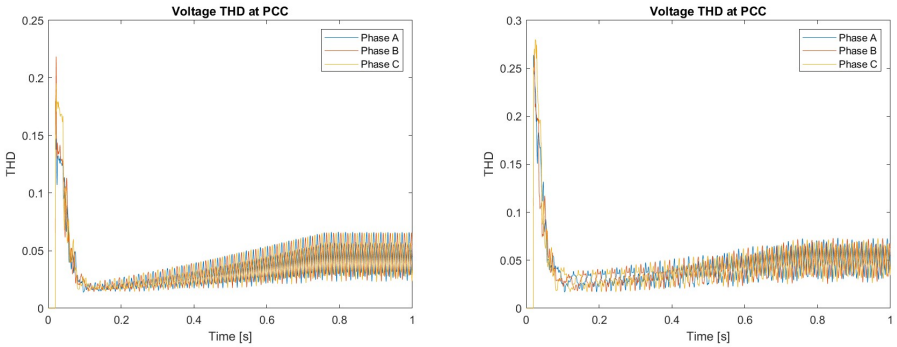

(a) A:1.10. (b) B:1.10.

Figure 43: Voltage THD at PCC in simulation cases A:1.10 & B:1.10.

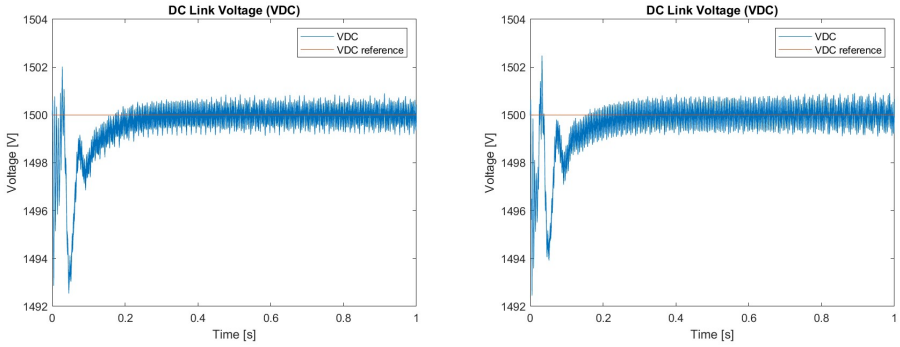

(a) A:1.10. (b) B:1.10.

Figure 44: DC link voltage in simulation cases A:1.10 & B:1.10.

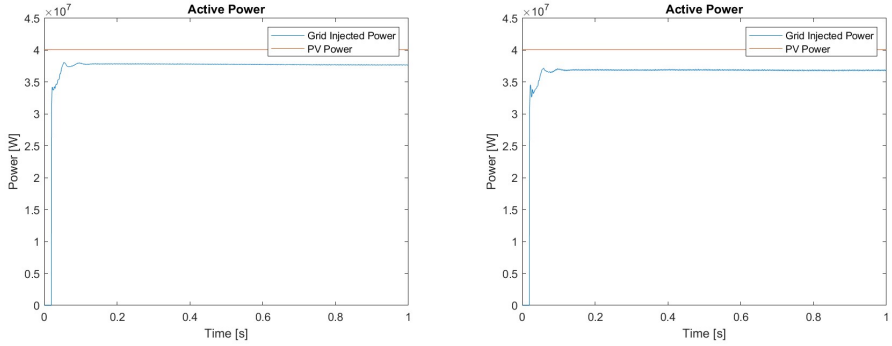

(a) A:1.10. (b) B:1.10.

Figure 45: Active power in simulation cases A:1.10 & B:1.10.

The PCC voltages , Fig. 42, are well behaved for both models apart from a distortion at the start of the simulation. Fig. 43 shows that this distortion is similar for the two cases but slightly more severe for the 20 transformer case. A similar situation appears in Fig. 44. Both controllers manage to follow their reference. Fig. 45 shows the active power into the grid. It is well behaved for both models with a slight difference at the start.

4.2 Stress Test

All four models were stress tested by reducing the SCR until system control failure. Control failure can be clearly seen in all the parameters measured. Herein only the PCC voltage will be presented. Illustrated in Figs. 46-49 is one plot (a) where the system is well behaved and one plot (b) where control failure occurs, for each model. The failure at around t = 0.05 s in all models is clearly visible. Fig. 50 compiles the results in a scatter plot.

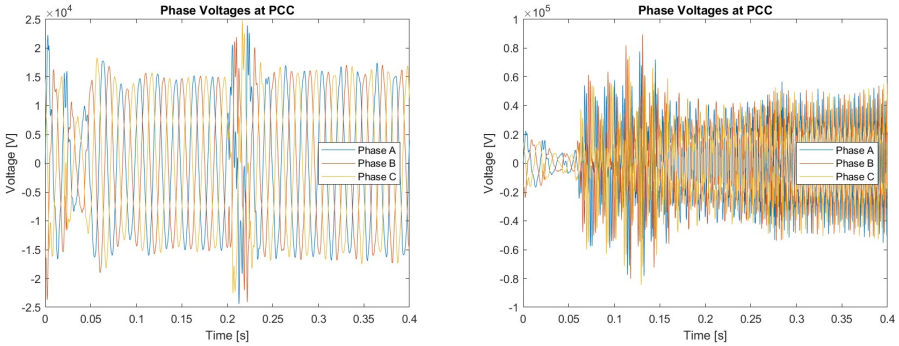

(a) A:2, SCR = 2.3. (b) A:2, SCR = 2.25.

Figure 46: Phase voltages at PCC in simulation case A:2.

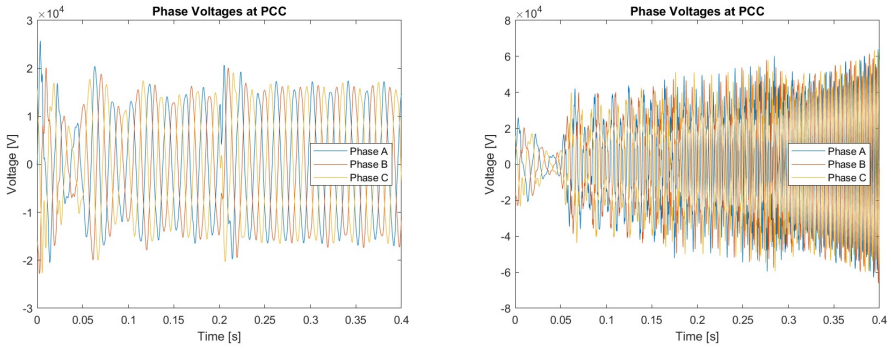

(a) B:2, SCR = 2.2. (b) B:2, SCR = 2.15.

Figure 47: Phase voltages at PCC in simulation case B:2.

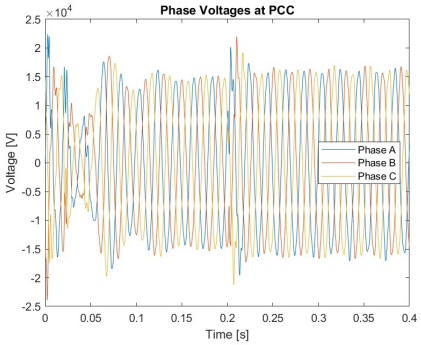

(a) C:2, SCR = 2.25.

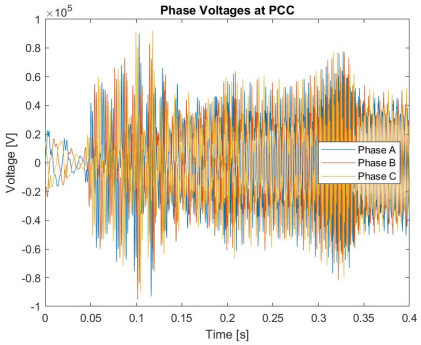

(b) C:2, SCR = 2.2.

Figure 48: Phase voltages at PCC in simulation case C:2.

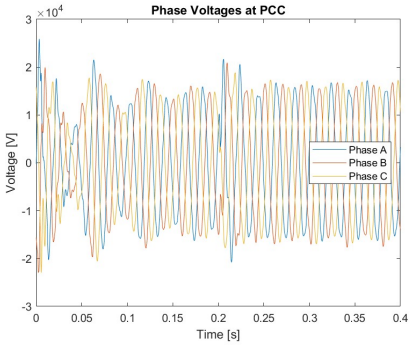

(a) D:2, SCR = 2.2.

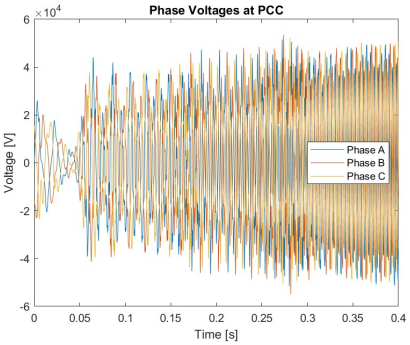

(b) D:2, SCR = 2.15.

Figure 49: Phase voltages at PCC in simulation case D:2.

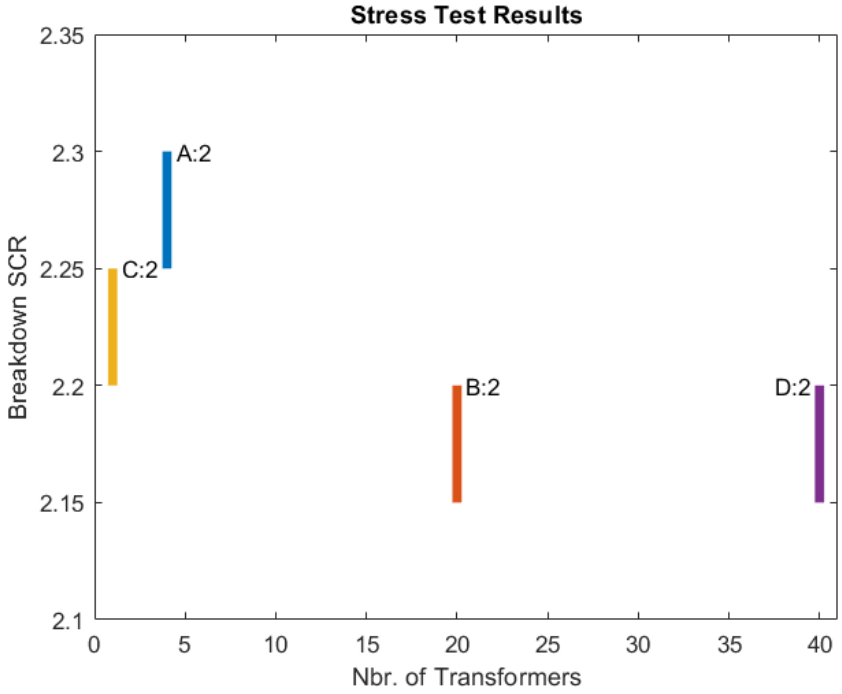

Figure 50: Scatter plot of the stress test.

As seen in the plots, there are small variations between the values of SCR which cause instability. However, there is no clear trend between the size/number of transformers and system resilience as illustrated in Fig. 50. Most resilient are the two models with the largest number of transformers, followed by the model with only one transformers and finally the model with four transformers.

5 Discussion

In this chapter the simulation results and the methodology used to build the simulation models and simulation cases will be discussed.

5.1 Discussion of the Simulation Results

General Performance Test

The PCC voltage along with the voltage THD indicates the quality of the power injected into the grid, the latter in terms of how perturbed the sinusoidals are. The THD voltage quantifies this perturbation and thus allows easy comparison between models. From the simulation results it can be seen that a weaker grid corresponds to the system becoming more sensitive to disturbances. This is explained by the fact that it means a larger impedance between the grid voltage and PCC, as such it is easier for the plant to impact the voltage. The change in solar irradiation seems to have a larger effect on the PCC voltage than the ramp in grid frequency. It should be noted that the ramp in THD seen during the ramp in grid frequency is a measurement error. The THD measurement block used in MATLAB Simulink is measuring at a fundamental frequency of 50 Hz. Thus, when the frequency deviates from 50 Hz, the non-50 Hz component increases and the THD rises without the system actually being more perturbed.

The voltage distortion varies between the models for different simulation cases. Cases 1.4 and 1.6 show a clear difference between the models, cases 1.2, 1.8 and 1.10 show a slight difference in between the models while 1.1, 1.3, 1.5, 1.7 and 1.9 show negligible difference between the models. For cases 1.4 and 1.6 the 20 x 2 MVA transformer model has a lower THD, while the 4 x 10 MVA transformer model has a lower THD for cases 1.2, 1.8 and 1.10. These results are somewhat strange. Longer cables causing a problem could be explained by the fact that they would cause a larger time delay in the system which makes the system harder to control. Why they would cause larger problems for one model than another and why the model with the worse behaviour varies from case to case is unclear.

When observing the DC link voltage, a quantity that indicates how well the control system performs, almost identical dynamics are apparent in both models, no matter the grid strength, cable length or disturbance. In the first tens of milliseconds they oscillate with the same frequency and amplitude. Taking a broader view, both of them approaches the reference value in a similar manner within the first few hundred milliseconds. The only difference

that can be distinguished is the transient response when the solar irradiation changes at 0.2 seconds, most apparent in case 1.3. Even here the difference in peak value is only in the order of one per thousand of the DC link voltage which does not diminish the fact that the DC link voltage is equally well controlled in both models, when exposed to the specific grid conditions and disturbances that have been studied in this work.

The active power is interesting to study and compare for two reasons; system efficiency and RFG compliance. Tab. 8 shows the system efficiency for the two models for a strong grid and short cables and for a strong grid and long cables. In the former case both models have an efficiency of about 97% while in the later model A's efficiency is about 95.7% and the model B's efficiency is about 92.4%. These differences can be explained by the cables. In case 1.1 the cables are short and thus they do not incur much losses. In case 1.2 they are very long and so the losses increase significantly. The difference in efficiency is a result of the fact that different cables dimensions are used for different models, where model A happens to have more over-dimensioned cables than model B. This was realized after the simulations were ran and unfortunately there was not enough time left to adjust the dimensioning.

As stated in Sec. 2.2.4 RFG requires that the plant is able to supply constant active power, equal to the reference value, independent of frequency changes. Both models managed this in the simulation cases where it was tested, i.e., the size and number of transformers does not compromise system compliance with this specific RFG requirement.

To summarize; the behaviour was very similar across all simulation cases and parameters tested. When there was a difference in the PCC voltage distortion the model with four transformers would perform better in some cases while the model with twenty transformer would perform better in others. That is, the general performance test showed no sign of the technical performance of a utility-scale PV plant depending on the number and size of transformers.

Stress Test

In the stress test, the twenty and forty transformer models performed equally and the best followed by the one transformer model and lastly the four transformer model performed the worst. Thus there is no trend between the number of transformers used and the lowest grid strength the system can handle. Furthermore, with the definition of a strong grid being SCR > 25 and that of a weak gird being SCR < 25, while the largest difference observed in the results between transformer setups is SCR $= 0.05$. That is, the difference observed is very small and can not with certainty be attributed to

the size and number of transformers. Other differences between the models exist, which could give rise to such small variations. I.e., the stress test showed no sign of the technical performance of a utility-scale PV plant being dependent on the number and size of transformers.

5.2 Discussion of the Methodology

In this section the method which was used will be discussed. Sec. 5.2.1 discusses the simulation model itself while Sec. 5.2.2 addresses the simulation cases.

5.2.1 Simulation Model

As stated in Ch. 3 the simulations were only carried out for one implementation of a utility-scale PV plant and, as stated in Ch. 2, these are implemented in a wide range of ways. Both in terms of hardware and software. Building an accurate model was the most time consuming part of the work and implementing it in a variety of ways is far beyond the scope of this work. This, in combination with the fact that the validity of this work on actual projects is dependent on how similar their implementation is to this one, is unfortunate. Hereafter some parts of the simulation model will be commented on.

The PI-controller generating a reactive power reference, labeled PI_4, was, as mentioned in Ch. 3, tuned entirely in an experimental manner. It was indeed a little less thought out than the other controllers, and it was not even obvious to use a PI-controller for this task. In fact it was not included from the start. In its place there was instead a constant zero reference for the i_q current. However, as reactive power is generated and consumed by inductive and capacitive elements in between the inverter and the PCC, zero reactive current at the inverter output does not guarantee zero reactive power injection to the grid, which is desirable in most situations[1]. Injecting reactive power to the grid proved to be problematic, especially when the grid was weak, as it had a large impact on the PCC voltage level. Hence, the controller was introduced to maintain close to nominal PCC voltage no matter the grid strength. It was tweaked until the purpose was fulfilled, but considering it was not even necessary to have in all simulation cases, not a lot of time was spent on tweaking it.

[1] An exception could be that the PV park is requested to help restoring the PCC voltage after a fault, regulated in RFG.

A lot of work was put into modelling the transformers in an accurate way, as they were the centerpiece of this work. Still some details, especially the magnetizing branch, were difficult to find values for as they are not clearly stated in datasheets and literature.

The leakage impedance X/R ratio was set to 20 for all the transformers used, a value based on a 10 MVA transformer according to [34]. After the simulations had been conducted, it was realized that the X/R ratio, according to [34], varies between 17.5 for a 3 MVA transformer to 30 for a 40 MVA transformer. Still, this inaccuracy is not believed to impact the validity of the results a lot. An X/R-ratio of for example 10, 20 or 40 results in almost the same reactance for a given impedance, and the reactive part of the transformer is the one potentially resulting in control problems and stability issues. This can be motivated with a calculation example, where $Z_{leakage} = 0.064\ p.u.$:

$$X/R = 10 \implies X_{leakage} = \frac{0.064}{\sqrt{1 + \frac{1}{10^2}}} = 0.06368\ p.u.$$
$$X/R = 20 \implies X_{leakage} = \frac{0.064}{\sqrt{1 + \frac{1}{20^2}}} = 0.06392\ p.u.$$
$$X/R = 40 \implies X_{leakage} = \frac{0.064}{\sqrt{1 + \frac{1}{40^2}}} = 0.06398\ p.u.$$

All three X/R-ratios results in reactance per unit values within less than half a percentage from each other. As a consequence it is much more important to model the leakage impedance value accurately than the X/R-ratio in this range, since the reactive part has a bigger impact on the behaviour than the resistive part. And these impedance values were set to realistic values as they were gathered directly from datasheets of real transformers.

As stated in Sec. 3.3.1 the DC-link voltage was set experimentally. It was found that the model had problems to output enough current to follow its references when it was set too low. An attempt at an explanation for this follows. Using natural sampling for the PWM it can output a maximum voltage level $V_{DC}/2$ [7], as such Eq. 26 sets the limit for the voltage which can be output at a phase, assuming the zero sequence voltage is zero. Note that while Eq. 26 is written for phase a, the same is true for the other phases if an appropriate phase shift is introduced to the trigonometric terms in the equation.

$$\hat{v}_{a-max} = V_{DC}/2 = v_d sin(\omega t) + v_q cos(\omega t) \tag{26}$$

Simplifying the plant to the inverter voltage on one end and the PCC voltage on the other with a equivalent impedance between them for the d- and q-components respectively as in Fig. 51 yields Eq. 27 and 28. Combining this with Eq. 26, the maximum output current, and thus the maximum output power, depends on V_{DC}. Provided this explanation is valid, it could also be used to set V_{DC} for utility-scale PV plants.

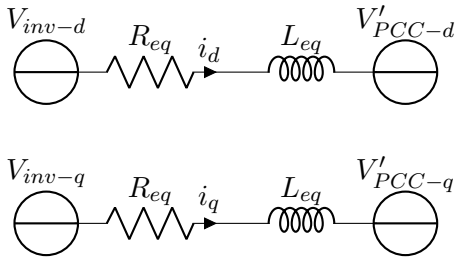

Figure 51: Simplification of a circuit diagram for the current flow into the grid from a VSI.

$$\begin{aligned} V_{inv-d} &= RI_d + \omega LI_q + V'_{grid-d} \Leftrightarrow \\ I_d &= \frac{V_{inv-d} - \omega LI_q - V'_{grid-d}}{R} \end{aligned} \tag{27}$$

$$\begin{aligned} V_{inv-q} &= RI_q - \omega LI_d + V'_{grid-q} \Leftrightarrow \\ I_q &= \frac{V_{inv-q} + \omega LI_d - V'_{grid-q}}{R} \end{aligned} \tag{28}$$

5.2.2 Simulation Cases

The outcome was not known when the simulation cases were formulated and only slight adjustments were made after running some test simulations. In hindsight, some decisions can be criticized.

The choice of simulating for only 0.4 seconds in many of the cases is questionable, as it is difficult to see if the THD has settled or not before the simulation ends. However, the amount of simulations along with the time each simulation required made the work very time consuming, even with the short simulation times. Some cases were simulated for a longer time, 1 second, to fully test a specific RFG requirement. Given more time for or more computational power longer simulation times would be an obvious choice.

Another choice that can be critiqued is that the two disturbances were only introduced one at the time and not together. A combination of the two disturbances is a realistic scenario, even though it is difficult to tell how common it is. The reason for not testing it was, once again, time constraints and an idea that it is more interesting to simulate cases that represent commonly occurring scenarios.

The purpose of the stress test was to get a quantitative measure of the robustness of each model. However, many parameters affect the robustness and the stress test was only performed on one pre-configured control system for each model. For every adjustment of the grid strength there might be an adjustment of the control parameters that helps maintaining the system stability. As a consequence the breakdown points should not be seen as the absolute truth but rather an indication on if there is a difference in robustness between the models.

6 Economical Comparison

In this chapter, a brief qualitative economical comparison of using different sizes and numbers of transformers will be conducted. Given the conclusions of Ch. 5, that the technical performance is independent of the size and number of transformers, it is of interest to analyse how the economics of the plant is affected by the number and size of transformers used. Such an analysis will be carried out in this chapter. As far as it is practical the analysis will be kept general.

A quantitative analysis would be hard to preform without a specific case. This analysis will therefore be conducted as a qualitative analysis, reasoning about the effects that a different number and size of transformers would have instead of trying the quantify what economical effects it would have. Three aspects will be considered; components and labour, logistics and redundancy and reliability.

6.1 Components and Labour

A change in the number of transformers in a utility-scale PV plant will cause changes in the number of other components used and the labour needed for installation. Transportation to the site will not be included in here and will be discussed in Sec. 6.2. To simplify the difference in components, the 4x10 MVA transformer setup and the 20x2 MVA transformer setup will be used as examples.

For the 4 x 10 MVA transformer setup, the components needed between the PCC and the low voltage switchgear would be:

- 4, 690 V, 10 MVA switchgear including
  - 10, 690 V, 1 MVA compartments
  - 1, 690 V, 10 MVA compartments including
    - 1, 690 V, 10 MVA Current transformer
    - 1, 690 V, 10 MVA Voltage transformer
    - 1, 690 V, 10 MVA Breaker
    - 1, 690 V, 10 MVA Disconnector
- 4, 0.69/20 kV, 10 MVA transformers
- 1, 20 kV, 40 MVA switchgear including
  - 4, 20 kV, 10 MVA compartments including
    - 1, 20 kV, 10 MVA Current transformer
    - 1, 20 kV, 10 MVA Voltage transformer
    - 1, 20 kV, 10 MVA Breaker
    - 1, 20 kV, 10 MVA Disconnector
  - 1, 20 kV, 40 MVA compartments including
    - 1, 20 kV, 40 MVA Current transformer
    - 1, 20 kV, 40 MVA Voltage transformer
    - 1, 20 kV, 40 MVA Breaker
    - 1, 20 kV, 40 MVA Disconnector

For the 20 x 2 MVA transformer setup, the components needed between the PCC and the low voltage switchgear would be:

- 20, 690 V, 2 MVA switchgear including
  - 2, 690 V, 1 MVA compartments
  - 1, 690 V, 2 MVA compartments including
    - 1, 690 V, 2 MVA Current transformer
    - 1, 690 V, 2 MVA Voltage transformer
    - 1, 690 V, 2 MVA Breaker
    - 1, 690 V, 2 MVA Disconnector
- 20, 0.69/20 kV, 2 MVA transformers
- 1, 20 kV, 40 MVA switchgear including
  - 20, 20 kV, 2 MVA compartments including
    - 1, 20 kV, 2 MVA Current transformer
    - 1, 20 kV, 2 MVA Voltage transformer
    - 1, 20 kV, 2 MVA Breaker
    - 1, 20 kV, 2 MVA Disconnector
  - 1, 20 kV, 40 MVA compartments including
    - 1, 20 kV, 40 MVA Current transformer
    - 1, 20 kV, 40 MVA Voltage transformer
    - 1, 20 kV, 40 MVA Breaker
    - 1, 20 kV, 40 MVA Disconnector

In summary, the total number of the following components are proportional to the number of transformers:

- Low voltage switchgear
- High power compartments in the low voltage switchgear
- Low power compartments in the high voltage switchgear

However, the power rating of these components is inversely proportional to the number of transformers. I.e., if the number of transformers increases by five, the number of these components also increases by five while their rating decreases to a fifth. Still according to [28] one component of a given rating is quite a bit cheaper than five components at a rating of one fifth of the

formerly mentioned one for pretty much all components within a somewhat common rating. This includes the transformers themselves. The number of transformers and components used also affects the amount of labour needed in all phases of a project's life-cycle. In the engineering and design phase, using a larger amount of transformers means more electrical design work and more protection- and control programming. In the construction phase it means more installation and assembly work, more oil pits have to be built and more cable tranches have to be dug. During operation every transformer requires checkups and maintenance, thus increasing the number of transformers will increase the time needed to be spent on this. In summary, there is a drastic increase of labour when using many small transformers in comparison to a few larger ones.

Concluding; from a components and labour point of view, using fewer larger transformers means a lower component cost and a lower labour cost.

6.2 Logistics

Onto the logistics aspect. One big part of it is transporting all parts of the PV plant to the project site. The weight of the transformers can be used as a measure to determine how difficult it is to transport them to remote areas with bad infrastructure. Weight and power-to-weight ratio approximations of a 2 MVA respectively a 10 MVA transformer, gathered from [36], are presented in Tab. 9. These are complemented with Fig. 52 and Fig. 53 which plots these values, and additional ones from [36], for a larger number of transformer ratings.

Table 9: Weight and power-to-weight-ratio for 2 MVA and 10 MVA transformers.

Trafo. Rating [MVA]	**Weight [ton]**	**Power-to-weight ratio [MVA/ton]**
2	5.2	0.39
10	14.9	0.67

The 10 MVA transformer is a factor 2.9 times heavier than the 2 MVA transformer. However, the 10 MVA transformer has a factor 1.7 larger power-to-weight ratio. In other words, the total weight of all transformers in PV plant will be smaller if 10 MVA transformer are used compared to if 2 MVA transformers are used. As seen in Fig. 52 and Fig. 53 the case of larger transformers being heavier while having a larger power-to-weigh ratio is general. Depending on the specific project, a higher weight of individual transformer could potentially be more problematic than a higher

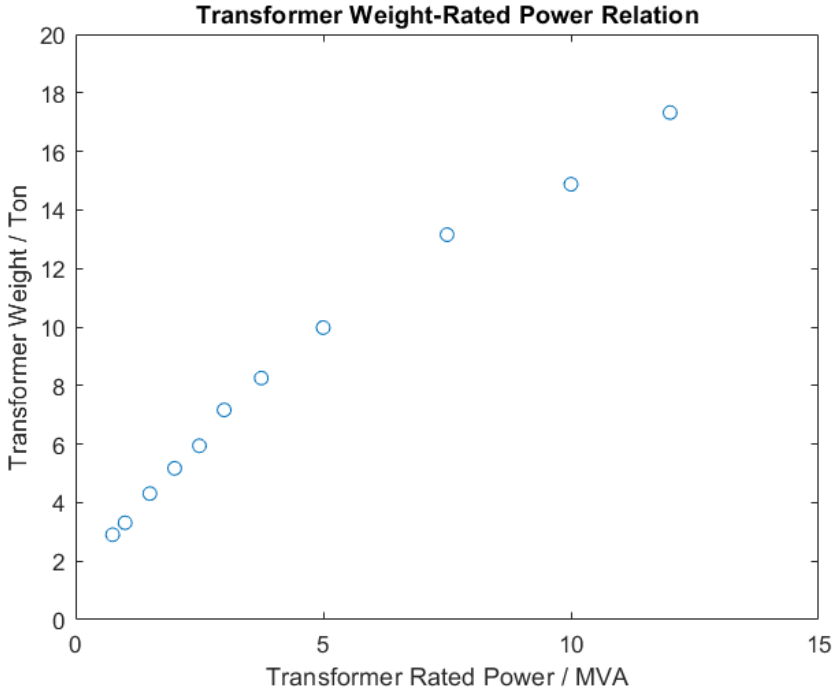

Figure 52: Relation between weight and rated power in transformers.

total weight of all transformers, or vice versa. For example, if the conditions of the site are such that the transport roads barely handles the load of a single 2 MVA transformer, using larger ones complicates the logistics quite a lot since it would require reinforcing roads or other solutions. If such a bottleneck does not exist, it makes more sense to prioritize 10 MVA transformers, from a weight perspective, as their higher power-to-weight ratio likely results in fewer total truck trips. In addition it is worth mentioning that the transformer may not even be the heaviest individual component in the power plant, meaning that the roads would have to be reinforced anyways. One such example could be if the PV plant is combined with batteries, serving as energy storage units, which comes in the form of containers that are possibly even heavier than the transformers.

Another interesting logistical aspect that will be examined is the leads times of the transformers. Exact lead times will not be provided as they are both difficult to find and constantly changing. However, as there is a big difference between small and large transformers, currently more than twice as long for 10 MVA compared to 2 MVA transformers [2], it is important to clarify the consequences of it. According to [37], long transformer lead times implies that 25 % of all global renewable energy projects are at risk of being delayed. A number which could be higher for renewable energy connected using larger

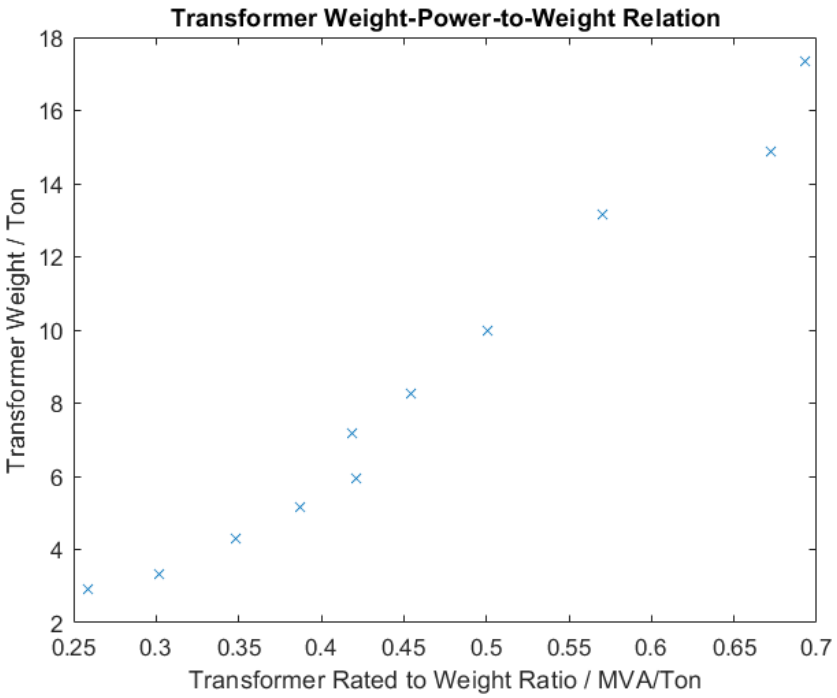

Figure 53: Relation between weight and power-to-weight ratio in transformers.

transformers since these have longer lead times. Project delays mean longer time to market which in turn means loss of revenue.

Thus, the logistics aspects do not clearly favour using neither smaller nor larger transformers, in the way that the components and labour aspect does. The weight aspect could favour either smaller or larger transformers and is entirely case dependent, while the lead times speak in favour of smaller transformers.

6.3 Redundancy and Reliability

Another aspect where it differs between using larger or smaller transformers is regarding the redundancy and reliability of the PV plant. If one single transformer fails, it will differ quite a lot in how much power that still can be fed into the grid and consequently the revenues, depending on the size and number of transformers in the plant. A 40 MW plant connected to 4x10 MVA transformers would result in a loss of 25% of the income if one of them fails, whereas the same plant connected to 20x2 MVA transformers would

result in a loss of 5%. In general it holds that the more transformers that are used, the more redundant and reliable the system is. The extreme case where the all PV power is connected to one transformer has no redundancy meaning that if the transformer fails no power can be fed into the grid and all income is lost until it is repaired or replaced. Tying this together with the discussion in 6.2 regarding lead times; a situation where a replacement is required would be very bad since it would cut all revenues for years.

7 Conclusions

In this chapter conclusions will be drawn, and they will be followed by some ideas for future work in Sec. 7.1 and contributions from the authors in Sec. 7.2.

Regarding the technical analysis; neither the general performance test or the stress test showed any significant connection between utility-scale PV plants technical performance and the size and number of transformers used. Thus, it opens up the possibility to consider the non-technical aspects when deciding on the size and number of transformers to use in a utility-scale PV plant.

Onto the economical comparison: the components and labour part promotes the use of a few, large transformers. The logistics aspect could favour either and is case dependent while the redundancy and reliability aspect favours many, small transformers.

The question-"What size and number of transformers should be used?" thus has the unsatisfactory answer-"It depends.". It depends on the case as well as on what is prioritized for the project. This work simply concludes that the technical performance is not significantly affected by the sizes and numbers of transformers and briefly discusses some economical advantages of using either a few large or many small transformers.

7.1 Future Work

A lot of interesting thoughts and ideas came up during this work. After spending so much time building an accurate model of a large-scale PV plant it was tempting to simulate more than what was in the scope of the work.

One concrete idea, which serves as a good complement to this study, is to do a more thorough economic analysis, for example by quantifying the economic performance of a fixed size PV plant with varying transformer size/number in a realistic case study.

One technical aspect that could be interesting to study is the behaviour during grid faults. In RFG the fault tolerance of power plant modules is regulated by low voltage ride through requirements, specifying whether or not the module has to stay connected and functioning depending on the PCC voltage profile. The main reason for excluding this from the scope was that it required implementation of specific fault techniques/algorithms, which was not a reasonable workload.

To verify the results of the simulations, similar tests could be performed in a lab environment. However, as the work involves very large and expensive components it might be difficult to get a fair representation of the simulations cases in a lab.

7.2 Contributions

The work has, through its entirety, been a close cooperation. In the case were work has been done by one person, it has been reviewed, and possibly edited, by the other. It is thus not deemed possible to distinguish which parts were done by whom without being petty.

8 Bibliography

[1] IEA, "Renewables 2023," Tech. Rep., 2024. [Online]. Available: https://iea.blob.core.windows.net/assets/96d66a8b-d502-476b-ba94-54ffda84cf72/Renewables_2023.pdf

[2] S. Harnestam, May. 2024, private communications.

[3] A. Cabrera-Tobar, E. Bullich-Massagué, M. Aragüés-Peñalba, and O. Gomis-Bellmunt, "Topologies for large scale photovoltaic power plants," *Renewable and Sustainable Energy Reviews*, vol. 59, pp. 309–319, 2016. [Online]. Available: https://www.sciencedirect.com/science/article/pii/S1364032116000289

[4] N. Mansouri, A. Lashab, D. Sera, J. M. Guerrero, and A. Cherif, "Large photovoltaic power plants integration: A review of challenges and solutions," *Energies*, vol. 12, no. 19, 2019. [Online]. Available: https://www.mdpi.com/1996-1073/12/19/3798

[5] M. H. Mohamed Hariri, M. K. Mat Desa, S. Masri, and M. A. A. Mohd Zainuri, "Grid-connected pv generation system—components and challenges: A review," *Energies*, vol. 13, no. 17, 2020. [Online]. Available: https://www.mdpi.com/1996-1073/13/17/4279

[6] N. H. Baharudin, T. M. N. T. Mansur, F. A. Hamid, R. Ali, and M. I. Misrun, "Topologies of dc-dc converter in solar pv applications," *Indonesian Journal of Electrical Engineering and Computer Science*, vol. 8, pp. 368–374, 2017.

[7] M. Alaküla, P. Karlsson, and H. Bängtsson, *Power Electronics - Devices, Converters, Control and Applications*, 2019.

[8] ONSEMI, "Igbt technologies and applications overview: How and when to use an igbt," ONSEMI, Tech. Rep., 2023.

[9] M. Hlaili and H. Mechergui, "Comparison of different mppt algorithms with a proposed one using a power estimator for grid connected pv systems," *International Journal of Photoenergy*, vol. 2016, pp. 56–65, 2016. [Online]. Available: https://api.semanticscholar.org/CorpusID:54786750

[10] K. Zeb, W. Uddin, M. Khan, Z. Ali, M. U. Ali, N. Christofides, and H. Kim, "A comprehensive review on inverter topologies and control strategies for grid connected photovoltaic system," *Renewable and Sustainable Energy Reviews*, vol. 94, pp. 1120–1141, 2018. [Online]. Available: https://www.sciencedirect.com/science/article/pii/S136403211830491X

[11] M. Memon, "Sizing of dc-link capacitor for a grid connected solar photovoltaic inverter," *Indian Journal of Science and Technology*, vol. 13, pp. 2272–2281, 06 2020.

[12] F. Blaabjerg, R. Teodorescu, M. Liserre, and A. Timbus, "Overview of control and grid synchronization for distributed power generation systems," *IEEE Transactions on Industrial Electronics*, vol. 53, no. 5, pp. 1398–1409, 2006.

[13] MathWorks, accessed: 2024-05-28. [Online]. Available: https://www.mathworks.com/help/sps/ref/parktransform.html

[14] F. Gardner, *Phaselock Techniques*. Wiley, 2005. [Online]. Available: https://books.google.se/books?id=r5yjPuWQde0C

[15] M. Collins, May 2024, private communications.

[16] A. Isaksson, "Model based control design," p. 2, 1999.

[17] L. B. G. Campanhol, S. A. O. da Silva, V. D. Bacon, and A. A. O. Junior, "Three-phase grid-connected pv system operating with feedforward control loop and active power-line conditioning using npc inverter," in *IECON 2016 - 42nd Annual Conference of the IEEE Industrial Electronics Society*, 2016, pp. 3099–3104.

[18] S. Zarei, H. Mokhtari, M. Ghasemi, S. Peyghami, P. Davari, and F. Blaabjerg, "Dc-link loop bandwidth selection strategy for grid-connected inverters considering power quality requirements," *International Journal of Electrical Power & Energy Systems*, vol. 119, p. 105879, 2020. [Online]. Available: https://www.sciencedirect.com/science/article/pii/S0142061519322082

[19] A. Reznik, M. G. Simões, A. Al-Durra, and S. M. Muyeen, "*lcl* filter design and performance analysis for grid-interconnected systems," *IEEE Transactions on Industry Applications*, vol. 50, no. 2, pp. 1225–1232, 2014.

[20] M. S. S. J. Duncan Glover, Thomas J. Overbye, *Power System Analysis & Design, Sixth Edition, SI*. Cengage Learning, 2016.

[21] K. N. D. Pejovski, D. Trajkovski, "Harmonic analysis of no-load current in distribution transformers," November 2016.

[22] MathWorks, accessed: 2024-05-29. [Online]. Available: https://www.mathworks.com/help/sps/powersys/ref/threephasepisectionline.html

[23] N. A. E. R. Corporation, "Short-circuit modeling and system strength," p. iv, 2018.

[24] K. U. Johan Olav Tande, Giuseppe Di Marzio, "System requirements for wind power plants," SINTEF Energy Research, Tech. Rep., 2007.

[25] H. Zumbahlen, "Chapter 1 - the op amp," in *Linear Circuit Design Handbook*, H. Zumbahlen, Ed. Newnes, 2008, pp. 1–82.

[26] O. J. of the European Union, "Commission regulation (eu) 2016/631 of 14 april 2016 establishing a network code on requirements for grid connection of generators," accessed: 2024-05-06. [Online]. Available: https://eur-lex.europa.eu/legal-content/EN/TXT/PDF/?uri=CELEX:32016R0631

[27] Energimarknadsinspektionen, "Energimarknadsinspektionens föreskrifter om fastställande av generellt tillämpliga krav för nätanslutning av generatorer eifs 2018:2," accessed: 2024-05-06. [Online]. Available: https://ei.se/download/18.5b0e2a2a176843ef8f5b74/1608639227153/EIFS-2018-2-om-faststC3%A4llande-av-generellt-tillC3%A4mpliga-krav-fC3%B6r-nC3%A4tanslutning-av-generatorer.pdf

[28] V. Lovén, Feb. - May 2024, private communications.

[29] "Ieee standard for harmonic control in electric power systems," *IEEE Std 519-2022 (Revision of IEEE Std 519-2014)*, pp. 1–31, 2022.

[30] ABB, "Abb 1 mva 20/10/0,4 kv," https://www.btbtransformers.com/transformer/abb-1-mva-20-10-04-kv/, accessed: 2024-04-22.

[31] ——, "Abb 2 mva 11,5/0,4 kv," https://www.btbtransformers.com/transformer/abb-2-mva-115-04-kv/, accessed: 2024-04-22.

[32] ——, "Abb 10 mva 33/11 kv dyn11," https://www.btbtransformers.com/transformer/abb-10-mva-33-11-kv-dyn11/, accessed: 2024-04-22.

[33] O. PTCL, "Technical specification for 40mva, 132/33 kv power transformer," https://optcl.co.in/writereaddata/Tender/103918113914Technical_specification_24052018.pdf, accessed: 2024-04-22.

[34] IEEE, *C37.010*, Std., 2016.

[35] NKT, "Mellanspänningskabel med pex-isolering," https://nkt.widen.net/content/iveqn7cqgj/pdf/230529_AXAL-TT-Pro-3_24kV.pdf?u=gj0n1y, accessed: 2024-05-6.

[36] Prolec, "Substation transformers," https://www.gevernova.com/grid-solutions/products/brochures/substation.pdf, accessed: 2024-05-15.

[37] A. B. S. Chopra, K. Jacobs and B. Boucher, Wood Mackenzie, Tech. Rep., 2024. [Online]. Available: https://go.woodmac.com/l/131501/2023-11-09/316xg5/131501/1699538868Yeh4yZTL/Power_transformers___Supply_Shortage_and_high_lead_times.pdf

Appendices

A Controller Settings

Tab. 10 presents all different PI-controller setting used in different simulation cases.

Table 10: Settings for the PI-controllers.

Trafo. Config.	**Cable Length [km]**	PI_1 & PI_2	PI_3	PI_4
1 x 40 MVA	10	P = 2.77 I = 133	P = 64.4 I = 1000	P = 0.16 I = 50
4 x 10 MVA	1	P = 2.10 I = 42	P = 64.4 I = 1000	P = 0.16 I = 50
4 x 10 MVA	10	P = 2.31 I = 126	P = 64.4 I = 1000	P = 0.16 I = 50
20 x 2 MVA	1	P = 2.01 I = 48.8	P = 64.4 I = 1000	P = 0.16 I = 50
20 x 2 MVA	10	P = 2.41 I = 210	P = 64.4 I = 1000	P = 0.16 I = 50
40 x 1 MVA	10	P = 2.77 I = 133	P = 64.4 I = 1000	P = 0.16 I = 50

B Supplementary Simulation Results

Presented below, in Figs. 54-73, are plots showing the results from all simulation cases that were left out from Sec. 4.

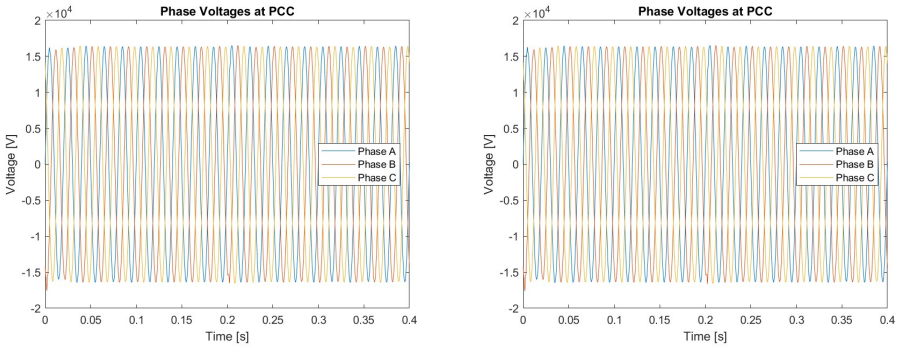

(a) A:1.1. (b) B:1.1.

Figure 54: Phase voltages at PCC in simulation cases A:1.1 & B:1.1.

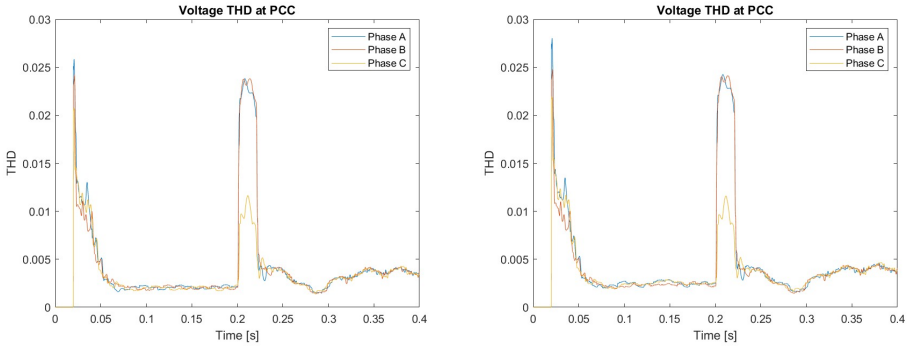

(a) A:1.1. (b) B:1.1.

Figure 55: Voltage THD at PCC in simulation cases A:1.1 & B:1.1.

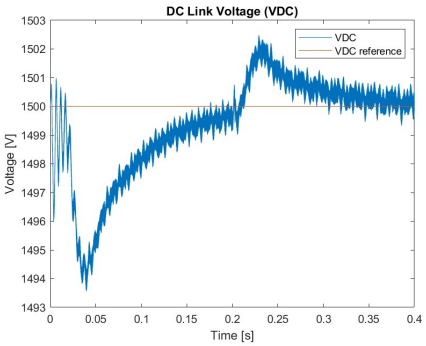

(a) A:1.1.

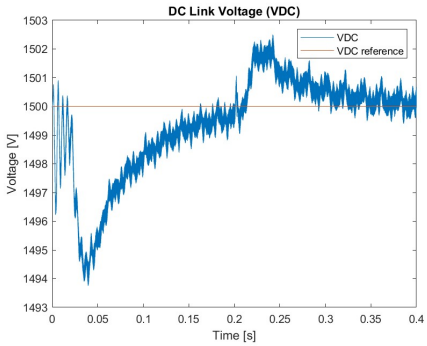

(b) B:1.1.

Figure 56: DC link voltage in simulation cases A:1.1 & B:1.1.

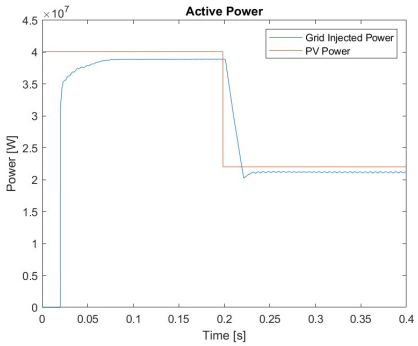

(a) A:1.1.

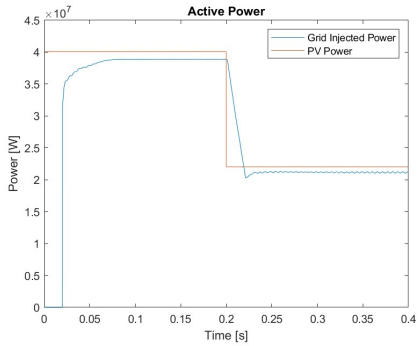

(b) B:1.1.

Figure 57: Active power in simulation cases A:1.1 & B:1.1.

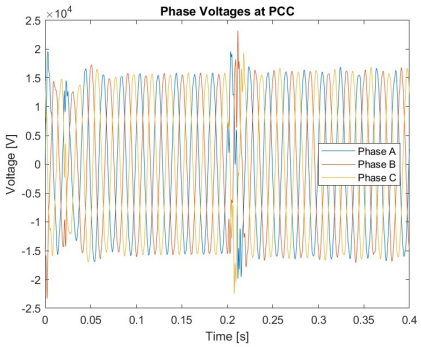

(a) A:1.3.

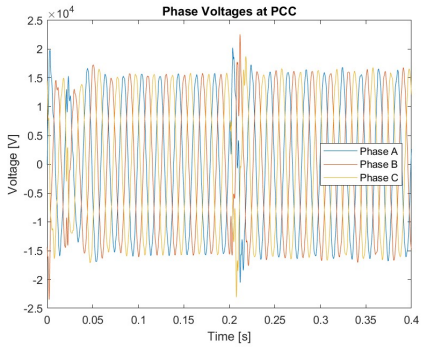

(b) B:1.3.

Figure 58: Phase voltages at PCC in simulation cases A:1.3 & B:1.3.

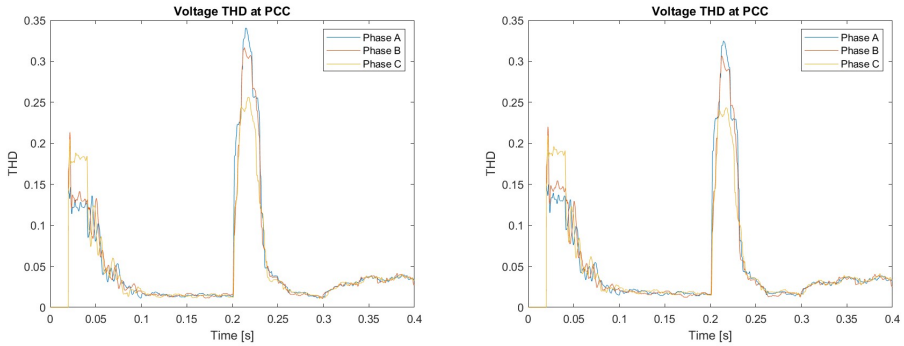

(a) A:1.3. (b) B:1.3.

Figure 59: Voltage THD at PCC in simulation cases A:1.3 & B:1.3.

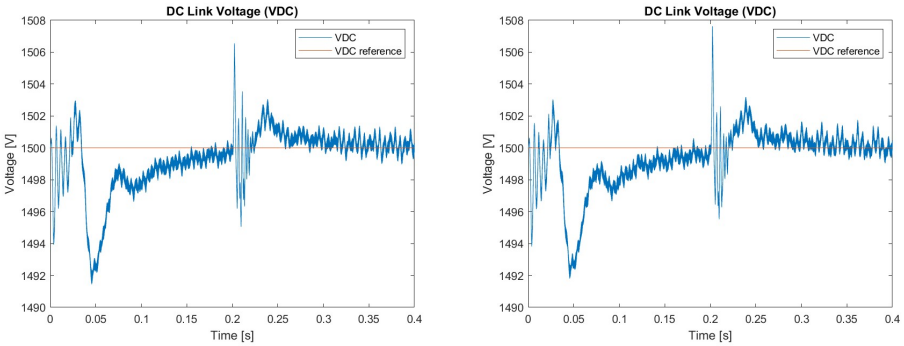

(a) A:1.3. (b) B:1.3.

Figure 60: DC link voltage in simulation cases A:1.3 & B:1.3.

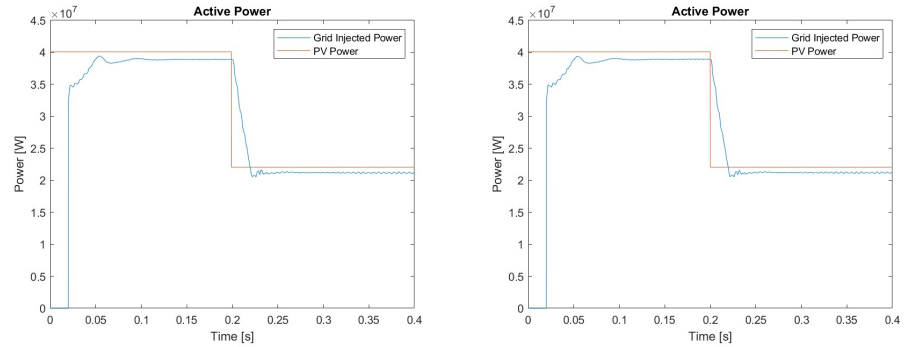

(a) A:1.3. (b) B:1.3.

Figure 61: Active power in simulation cases A:1.3 & B:1.3.

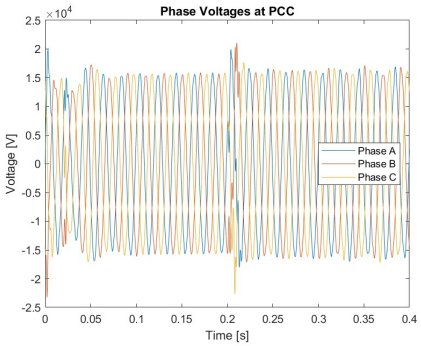

(a) A:1.5.

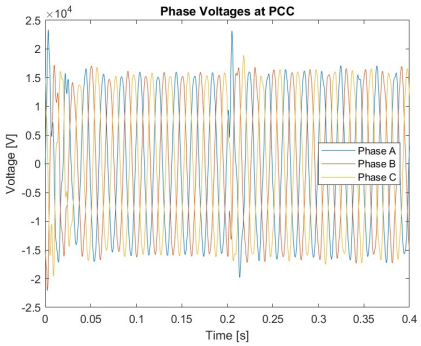

(b) B:1.5.

Figure 62: Phase voltages at PCC in simulation cases A:1.5 & B:1.5.

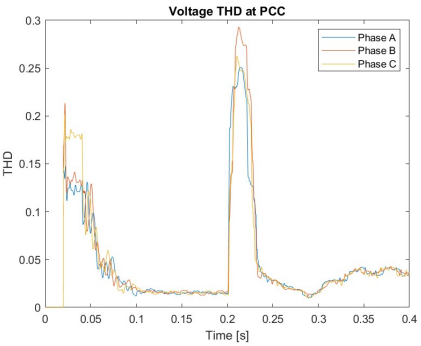

(a) A:1.5.

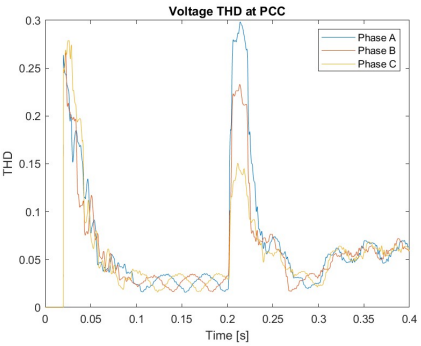

(b) B:1.5.

Figure 63: Voltage THD at PCC in simulation cases A:1.5 & B:1.5.

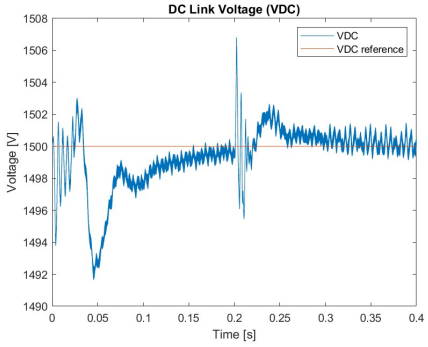

(a) A:1.5.

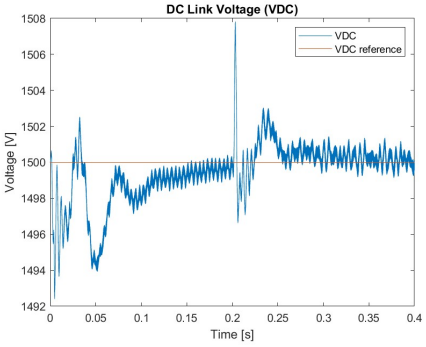

(b) B:1.5.

Figure 64: DC link voltage in simulation cases A:1.5 & B:1.5.

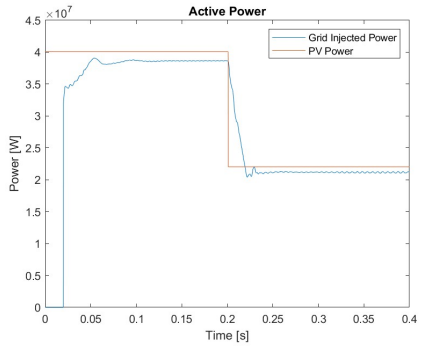

(a) A:1.5.

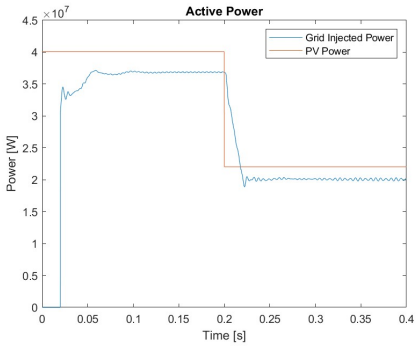

(b) B:1.5.

Figure 65: Active power in simulation cases A:1.5 & B:1.5.

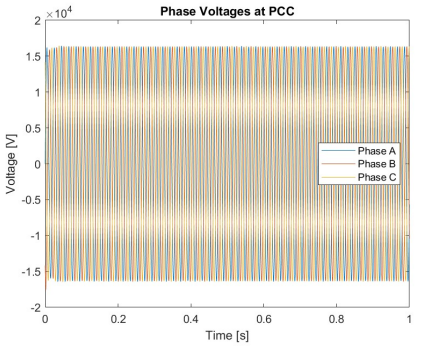

(a) A:1.7.

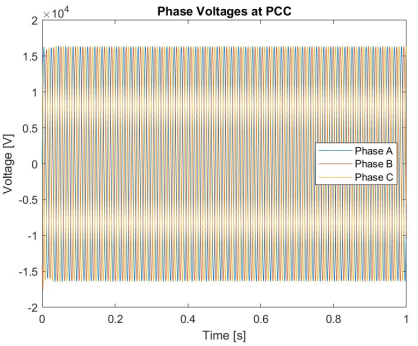

(b) B:1.7.

Figure 66: Phase voltages at PCC in simulation cases A:1.7 & B:1.7.

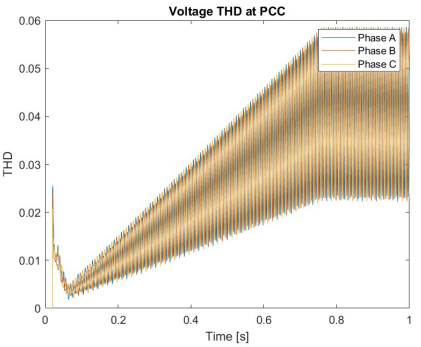

(a) A:1.7.

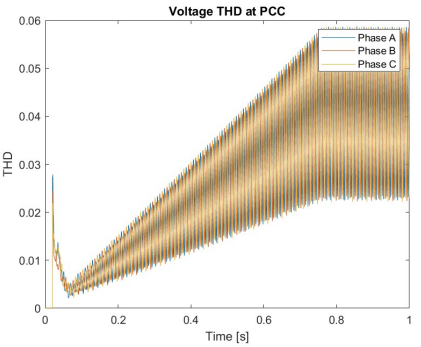

(b) B:1.7.

Figure 67: Voltage THD at PCC in simulation cases A:1.7 & B:1.7.

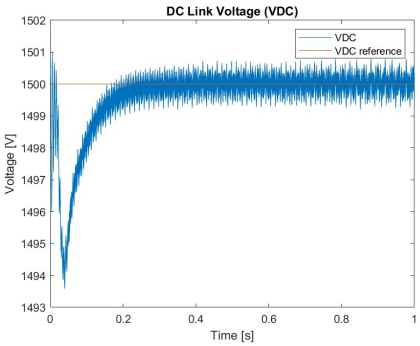

(a) A:1.7.

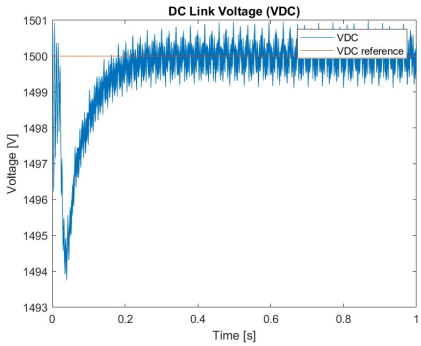

(b) B:1.7.

Figure 68: DC link voltage in simulation cases A:1.7 & B:1.7.

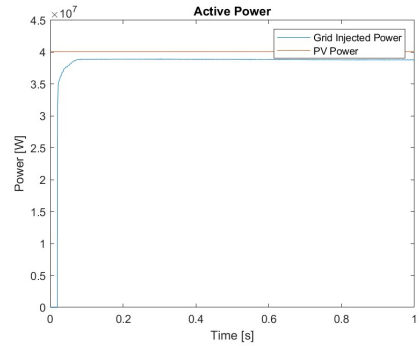

(a) A:1.7.

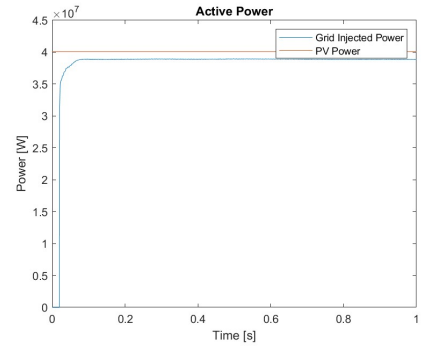

(b) B:1.7.

Figure 69: Power output in simulation cases A:1.7 & B:1.7.

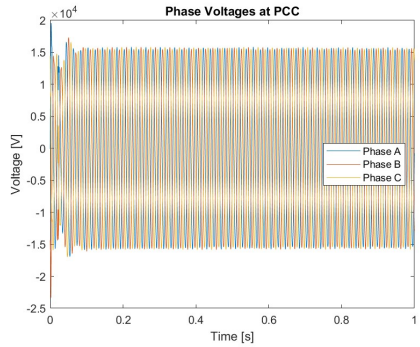

(a) A:1.9.

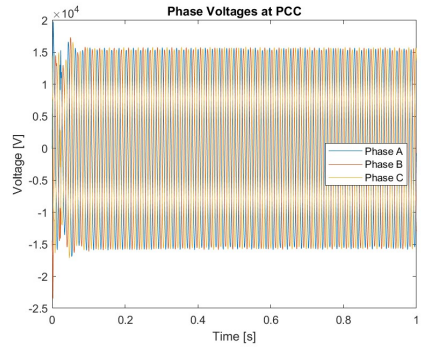

(b) B:1.9.

Figure 70: Phase voltages at PCC in simulation cases A:1.9 & B:1.9.

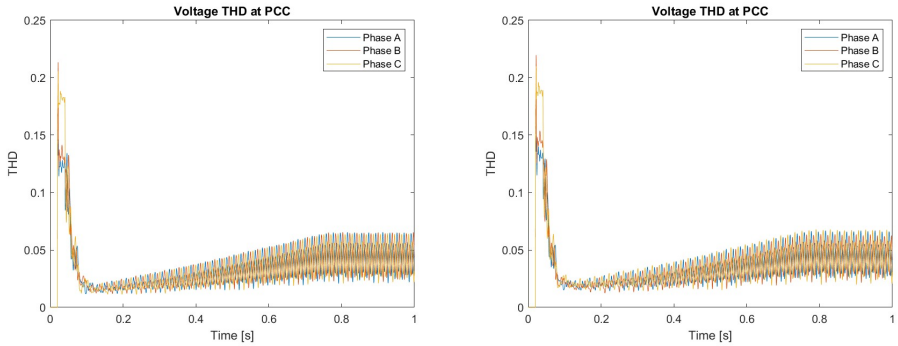

(a) A:1.9. (b) B:1.9.

Figure 71: Voltage THD at PCC in simulation cases A:1.9 & B:1.9.

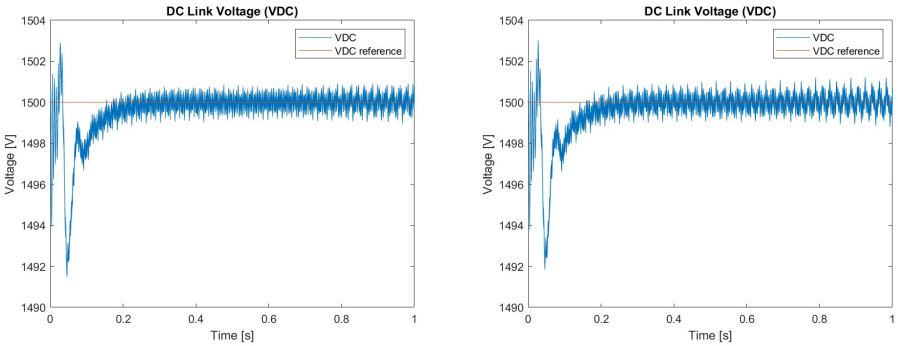

(a) A:1.9. (b) B:1.9.

Figure 72: DC link voltage in simulation cases A:1.9 & B:1.9.

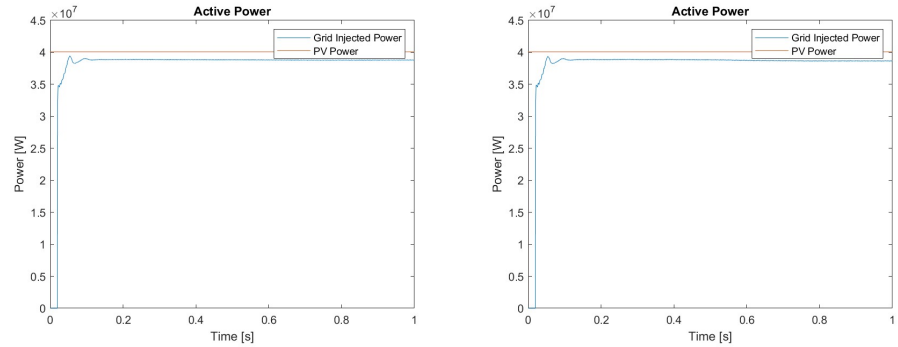

(a) A:1.9. (b) B:1.9.

Figure 73: Power output in simulation cases A:1.9 & B:1.9.